land

MDPI

Article

Investigating the Effects of Mining on Ecosystem Services in Panzhihua City: A Multi-Scenario Analysis

Xuanmiao Peng [1,2], Xiaoai Dai [1,2,3,*], Ryan Shi [4], Yujian Zheng [1,2], Xinyue Liu [1,2], Yuhe Xiao [1,2], Weile Li [1], Yang Zhang [2,3], Jue Wang [3,5] and Huan Huang [3,5]

[1] State Key Laboratory of Geohazard Prevention and Geoenvironment Protection, Chengdu University of Technology, Chengdu 610059, China; pengxuanmiao@stu.cdut.edu.cn (X.P.)
[2] College of Geography and Planning, Chengdu University of Technology, Chengdu 610059, China
[3] Digital Hu Huanyong Line Research Institute, Chengdu University of Technology, Chengdu 610059, China
[4] Worcester Polytechnic Institute, Worcester, MA 01609, USA
[5] College of Business, Chengdu University of Technology, Chengdu 610059, China
* Correspondence: daixiaoa@cdut.edu.cn

Abstract: Ecosystem services are fundamental for the sustainable management of urban environments, particularly in mining cities confronting unique socio-environmental complexities. This study explores the intricate interactions among ecosystem services in a representative mining city, focusing on the impact of mining activities. A novel approach is employed to introduce a comprehensive framework for scenario-based analysis of ecosystem services. Land use and ecosystem service values for 2050 were predicted under the following three scenarios: natural development, ecological protection, and farmland protection. Through the evaluation of four key ecosystem services, namely water yield, habitat quality, carbon storage, and soil conservation, ecosystem service bundles were identified, and the trade-offs and synergies among these bundles were explored. Moreover, ecosystem service bundles in the mining areas were analyzed compared to the region at large, underscoring how the mining of various mineral types distinctly influenced ecosystem services. The results showed a persistent decline in total ecosystem service values of the whole region during 2000–2020 due to the diminishing forest cover and the enlargement of farmland and impervious surfaces. Mining areas exhibited significant impacts, with the soil erosion bundle predominating. However, the soil erosion bundle significantly reduced in the granite, copper, and nickel mining areas. By 2050, total ecosystem service values are projected to slowly rise, except under the farmland protection scenario. The entire region is expected to be mostly occupied by the ecological vulnerability bundle. But the ecosystem vulnerability bundle of mining areas is projected to decrease, especially under the ecological protection scenario, highlighting the importance of conservation efforts. These changes will enhance the synergies between soil conservation and other ecosystem services.

Keywords: land use change; ecosystem services; ecosystem service value; ecosystem service bundles; trade-offs and synergies; mining city

check for updates

Citation: Peng, X.; Dai, X.; Shi, R.; Zheng, Y.; Liu, X.; Xiao, Y.; Li, W.; Zhang, Y.; Wang, J.; Huang, H. Investigating the Effects of Mining on Ecosystem Services in Panzhihua City: A Multi-Scenario Analysis. *Land* **2024**, *13*, 819. https://doi.org/10.3390/land13060819

Academic Editors: Wanxu Chen, Jie Zeng and Shuai Zhou

Received: 15 May 2024
Revised: 31 May 2024
Accepted: 4 June 2024
Published: 7 June 2024

Copyright: © 2024 by the authors. Licensee MDPI, Basel, Switzerland. This article is an open access article distributed under the terms and conditions of the Creative Commons Attribution (CC BY) license (https://creativecommons.org/licenses/by/4.0/).

1. Introduction

Ecosystem services (ESs) are ecological features, functions, and processes with a substantial contribution to human welfare [1,2]. Over the last half century, the Earth's ecosystem services are estimated to have declined by around 60% overall, due to the relentless increases in global population, industrialization, and urbanization [3]. Safeguarding the valuable resources only available through ecosystem services has now become a pressing challenge [4].

In order to stop the decline of ESs, researchers investigated the spatiotemporal fluctuations of these services and the interactions between them [5]. Trade-offs, synergies, and bundling are commonly observed interactions among ESs [6]. A trade-off happens when the improvement of one ES coincides with the reduction of another, whereas the synergy

exists when two ESs are mutually strengthened [7–10]. In 2007, Kareiva et al. [3] introduced the notion of ecosystem service bundles (ESBs) as a means of explaining the interactions between ecosystem services. ESBs are characterized as groupings of ESs that repeatedly co-occur across different spatial and temporal dimensions [11,12]. These dominant ESs are used to form bundles, which then allow for a deeper exploration of the relationships among these ESs [13,14]. A variety of models have been developed to quantify ESs . The CASA model [15], the RULSE model [16], the SWAT model [17,18], the SolVES model [19], and the InVEST model [20] have provided insights into ESs and their interactions. Compared to the CASA model focused on carbon cycling, the RULSE model focused on soil erosion, the SWAT model focused on hydrology and water quality, and the SolVES model focused on social value quantification, the InVEST model offers several advantages. It excels in multi-functionality, ease of use, adaptability, and comprehensive analysis. These features make the InVEST model suitable for holistic evaluations of ESs. After accessing ESs, researchers used clustering approaches to identify ESBs, such as the self-organizing map approach [21,22] and the K-means clustering algorithm [23–27]. Orsi et al. [28] evaluated the trade-offs and synergies between ESs, identifying the distribution of ESBs throughout the European Union and its Member States. However, existing studies often view ESs interactions statically [29,30], overlooking dynamic changes under future policies. Historical data may not accurately predict the complex dynamics of future ESs, possibly leading to inappropriate policy decisions [31,32]. Thus, simulating evolving interactions among ESs is vital in guiding sustainable ecosystem management.

Using model simulation and scenario analysis for evaluation of future ecosystem service changes offers a new approach to uncover ecosystem service dynamics under land use/land cover (LULC) [33]. In addition, changes in land use have a significant impact on ESs [34–36]. Therefore, researchers cannot study ESs without also taking LULC into account. Land use simulation models principally aim to forecast alterations in the spatial distribution and land quantity structure. The main quantitative structure prediction models are the Markov model and the SD model [37], while spatial distribution prediction models involve the CLUE-S model [38], the FLUS model [39,40], and the CA-Markov model [41], among others. Quantitative structure prediction models primarily quantify the variations in different land use categories [37]. However, the FLUS model and the CA model encounter notable obstacles in dynamically simulating patch-level changes across diverse land use categories, particularly in natural landscapes including forests and grasslands [42]. Liang et al. [43] developed the PLUS model to enhance land use simulations and offer insights for sustainable planning in 2021. The PLUS model, an advanced hybrid spatial model, originated from the enhanced FLUS model. It specializes in identifying driving factors behind diverse landscapes, employing an adaptive inertia competition mechanism for precise land use change probabilities. This results in high simulation fidelity and rapid data processing for complex land type evolution [44,45].

Mining has a substantial role in the world economy, representing 1.2% of the total global gross domestic product [46,47]. However, extraction of mineral resources can trigger the displacement or alteration of natural ecosystems, leading to ecological challenges including biodiversity loss and land degradation [48]. As a result, these phenomena, which are pronounced in mining landscapes, reduce the supply of ESs. Furthermore, the effects on ESs differ in both intensity and scope, contingent upon the nature and stage of mining activities [49–51]. China stands as the world's largest developing nation and the epicenter of mining activities in terms of concentration [52]. A quarter of its urban areas are classified as mining cities. Mining cities frequently grapple with deteriorating environmental issues and are prone to decline due to the depletion of non-renewable natural resources [53]. But there is currently a dearth of comprehensive frameworks for assessing the impact that mining different types of minerals has on ESs. Studies on mining and ESs tend to either concentrate on the effects of mining a single type of mineral or the effects of mining activities on a solitary ES [30,54]. Since mining is a principal economic endeavor in mining

cities, it is of paramount importance to address the issue of avoiding and reducing its influence on ESs [55,56].

In this study, the integrated PLUS-InVEST model was applied to predict LULC and ESs in Panzhihua city, spanning historical and future multi-scenario analysis. We first identified distinct ecosystem service bundles. Subsequently, we explored trade-offs and synergies between ESs across different bundles. Moreover, we analyzed the ESBs of different mineral resources across various scenarios to further explain the intricate interactions of ecosystem services in the mining areas. We hope that our research can serve as a basis for new policies in mining cities that balance advancements in mining with ecological preservation.

2. Materials and Methods

2.1. Study Area

Panzhihua, located at coordinates 26°05′–26°21′ N and 101°08′–102°15′ E, marks the southernmost region of Sichuan Province and shares a border with Yunnan Province (Figure 1). More specifically, it lies in the south–central region of the Panxi Rift Valley, with a terrain that slopes from northwest to southeast. Panzhihua experiences a blend of southern subtropical and northern temperate climates. The yearly precipitation is around 950 mm, and the mean year-round temperature is roughly 20.8 °C. Covering an area of 7414 square kilometers, the city accommodates a population surpassing 1.2 million individuals. Panzhihua, being a typical mining city in China, holds a substantial quantity of mineral resources. It holds 7.18 billion tonnes of vanadium-titanium magnetite, a type of iron ore. The vanadium titanium magnetite deposits of Panzhihua make up 72.3% of Sichuan's iron ore. The reserves of associated titanium resources account for 93% of the national total, ranking first globally. The reserves of associated vanadium resources account for 63% of the national total, ranking third globally. This scale of mining activities, unsurprisingly, has grave geological and ecological consequences. Panzhihua faces mudslides, landslides, soil erosion, vegetation decline, and soil contamination to the great detriment of its people [57]. Therefore, mining must be managed in Panzhihua, lest the city become unlivable due to ecological disaster.

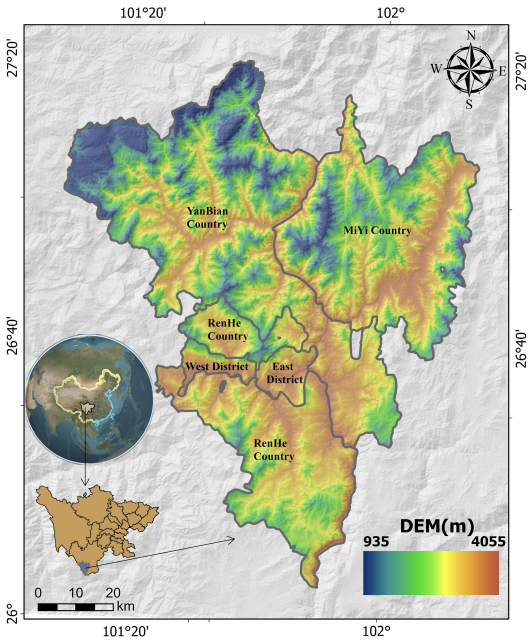

Figure 1. Overview map of study area.

2.2. Data Sources

We primarily dealt with three types of data, namely raster data, vector data, and text data, all processed within the scope of Panzhihua city. Mineral resource data were provided

by the Sichuan Comprehensive Geological Survey Institute (http://www.scddy.com.cn/) and accessed on 3 November 2023. Meteorological data were sourced from the National Earth System Science Data Center (https://www.geodata.cn) and accessed on 17 September 2023. Table 1 provides a comprehensive summary of the data information. ArcGIS Pro 3.1 software was employed for the processing of selected datasets, enabling the delineation of the Panzhihua watershed via hydrological analysis tools applied to DEM data. Additionally, the slope raster was extracted from DEM data. Subsequently, the computation of Euclidean distances yielded the generation of gridded distance data of mines, secondary and tertiary roads, railways, expressways, watersheds, governmental entities, and railway stations. For consistency, the geographic coordinate system was standardized to WGS_1984_Zone_48N. At a resolution of 30 × 30 m, the raster data underwent resampling.

Table 1. Data details table.

Data Name	Data Format	Data Sources
LULC data	Grids at 30 m resolution	https://zenodo.org/record/4417810#.YxhwS6HiviD (accessed on 24 September 2023)
DEM data		https://www.gscloud.cn/search (accessed on 5 September 2023)
Precipitation data Temperature data Evapotranspiration data		https://www.geodata.cn (accessed on 17 September 2023)
Soil type data	Grids at 1 km resolution	https://data.tpdc.ac.cn (accessed on 23 October 2023) [58] https://www.fao.org (accessed on 4 November 2023)
GDP Population density		https://www.resdc.cn/DOI (accessed on 25 October 2023)
Soil property dataset for land surface modeling across China	Grid at 30 arc-second resolution	http://poles.tpdc.ac.cn (accessed on 29 October 2023)
Secondary roads Tertiary roads Class IV roads Motorways Railways High-speed rail stations Government sites Water bodies	Vector data	https://www.webmap.cn/commres.do?method=result100W (accessed on 11 November 2023)
Monitoring data from mining environments in Sichuan Province	Text data	http://www.scddy.com.cn/ (accessed on 3 November 2023)
Panzhihua Statistical Yearbook		http://tjj.panzhihua.gov.cn/zwgk/tjsj/tjnj2022/index.shtml (accessed on 26 November 2023)
China Yearbook of Agricultural Product Price Surveys		https://cnki.nbsti.net/CSYDMirror/Trade/home/index/Z009 (accessed on 2 December 2023)

2.3. Methodology

We incorporated the PLUS-InVEST model to forecast future variations in LULC and ESs across multiple scenarios. Specifically, we evaluated crucial ecosystem services through the InVEST model. These services were evaluated across various scenarios targeting the year 2050. Subsequently, we normalized these ESs and employed the K-means clustering method to identify the ESBs. The correlation coefficients were calculated between ESBs in order to find any potential trade-offs or synergies (Figure 2).

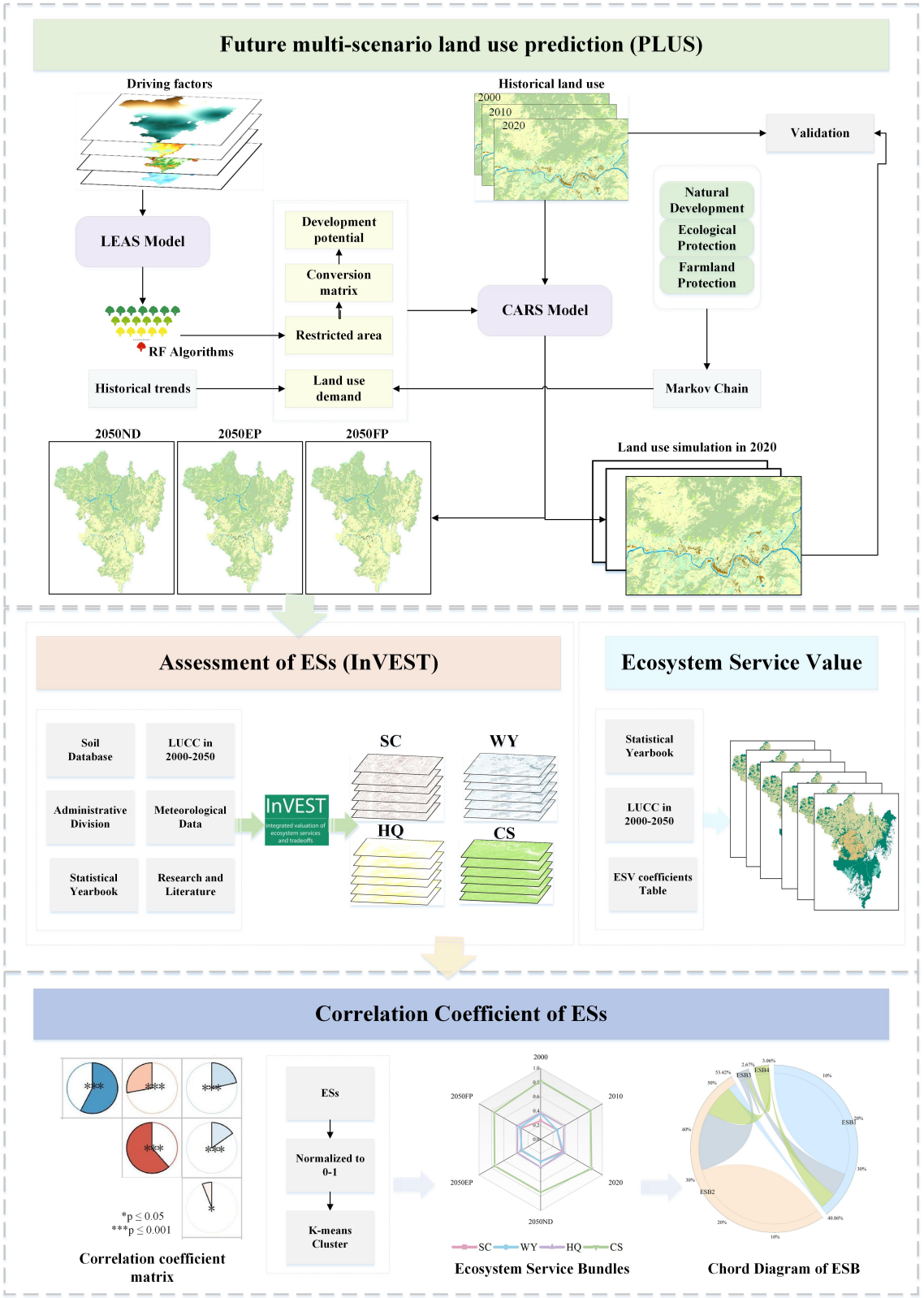

Figure 2. Flowchart. HQ: habitat quality; WY: water yield; CS: carbon storage; SC: soil conservation; EP: ecological protection scenario; ND: natural development scenario; FP: farmland protection scenario.

2.3.1. Simulation of LULC across Multiple Scenarios

(1) PLUS Model

The two core components of the model are a rule-mining framework utilizing a land expansion analysis (LEAS) approach and cellular automaton (CA) employing multi-type random patch seeds (CARS) [43]. The LEAS identifies changing areas of LULC between two time periods and assesses the impact levels of land use categories and driving factors with the Random Forest Classification (RFC) algorithm. The CARS module incorporates both "top-down" and "bottom-up" mechanisms into its CA model. It is applied to forecast future land cover requirements by employing an adaptable coefficient and simulating spatial–temporal transformations in a dynamic manner, contingent upon the likelihood of development.

(2) Multi-scenario Settings

In the PLUS model, we further implemented multi-scenario settings. Based on the Markov chain and historical land use change trends, we integrated relevant studies to determine land use demand under different scenarios by adjusting the transition probabilities for specific land use categories. Subsequently, the land use demand and driving factors (Figure A1 in Appendix A) were input into the LEAS module to assess their development potential. By integrating land use demand, restricted areas, the conversion matrix, and development potential, the CARS module projected the spatial distribution of land use by 2050 in Panzhihua city. The descriptions of different scenarios and the specific parameter settings are detailed as follows.

The natural development (ND) scenario serves as the basis for simulating other scenarios without setting the conversion matrix among various types of LULC [43]. The Markov chain was used in the PLUS model to forecast land use demand by analyzing the land use change rate from 2010 to 2020.

The ecological protection (EP) scenario emphasizes preserving the ecosystem by severely restricting impervious development to achieve the greatest environmental benefits [42]. The likelihood of forests, water, and grasslands being transformed into alternative land use categories is diminished [59,60].

The farmland protection (FP) scenario regulates the conversion of farmland to impervious surfacesby establishing permanent vital farmland protection regions as spatial restrictions and adds chances of transferring other land use categories into farmland [42].

(3) Model Validation

The simulated results of the model were evaluated using an Overall Accuracy (OA) index. Furthermore, we applied the Figure of Merit (FoM) coefficient to calculate the precision of the outcomes. This was done by comparing the variations in the simulation with the variations observed between 2010 and 2020 [61]. The FoM coefficient [62] is calculated as follows:

$$\text{FoM} = \frac{\text{Hits}}{\text{Wrong hits} + \text{Misses} + \text{Hits} + \text{False alarms}} \quad (1)$$

where false alarms are pixels simulated as unchanged but observed as changed, misses are pixels simulated as changed but observed as unchanged, hits are pixels simulated and observed as changed, and wrong hits are pixels that are both simulated and observed as changed but categorized as errors in the simulation.

2.3.2. Evaluation of Ecosystem Services (InVEST)

(1) Soil Conservation (SC)

The sediment delivery ratio model [63] in the InVEST model was used to compute SC by subtracting the RKLS from the USLE, taking into account land use category, soil, and climate data. The structure of the equation is expressed as follows:

$$USLE_j = R_j \times K_j \times LS_j \times C_j \times P_j \quad (2)$$

$$RKLS_j = R_j \times K_j \times LS_j \quad (3)$$

$$SC_j = RKLS_j - USLE_j \quad (4)$$

where $USLE_j$ represents the total potential soil loss in the original land cover at grid j (t/hm^2); $RKLS_j$ represents the potential for all soil loss for bare soil at grid j (t/hm^2); SC_j represents the actual soil conservation at grid j (t/hm^2); R_j represents the factor of rainfall erosion; K_j represents the factor of soil erosion susceptibility, which is calculated using the EPIC method; LS_j represents the factor of the slope length and gradient; C_j represents the factor pertaining to the management of vegetation cover; and P_j represents the factor related to procedural support.

(2) Water Yield (WY)

The water yield module combines various parameters, including rainfall, transpiration of vegetation, evaporation from surfaces, available vegetation water content, soil depth, and other properties [64,65]. The Budyko hydrothermal coupling equilibrium hypothesis is used to consider these aspects. The structure of the equation is expressed as follows:

$$Y_{jx} = \left(1 - \frac{AET_{jx}}{P_{jx}}\right) P_{jx} \quad (5)$$

$$\frac{AET_{jx}}{P_{jx}} = \frac{1 + w_x R_{jx}}{1 + w_x R_{jx} + \frac{1}{R_{jx}}} \quad (6)$$

$$w_x = Z\frac{AWC_{jx}}{P_{jx}} \quad (7)$$

$$R_{jx} = \frac{k_{jx} ETO_{jx}}{P_{jx}} \quad (8)$$

where Y_{jx} represents the yearly water yield at grid j of land use category x (mm); AET_{jx} represents the actual average annual evapotranspiration at grid j of land use category x (mm); P_{jx} represents the current evapotranspiration at grid j of land use category x; R_{jx} represents the Budyko aridity index at grid j of land use category x; w_x represents the annual water demand of plants and the total volume of precipitation delivered in a year; k_{jx} represents the coefficient of vegetation evapotranspiration at grid j; ETO_{jx} represents the mean yearly potential evapotranspiration at grid j of land use category x (mm); AWC_{jx} represents the existing soil level of moisture on grid j of land use category x, which is controlled by factors such as soil depth and texture; and Z represents a variable that changes with the seasons and represents the amount and pattern of rainfall, which differ in various research locations.

(3) Habitat Quality (HQ)

The habitat quality module incorporates spatial and non-spatial data inputs, such as LULC data, threat sources, habitat categories, and their respective sensitivities [66,67]. It combines these factors to calculate suitability and degradation on a scale of 0 to 1, with higher values indicating better habitat conditions and lower levels of human disturbance. We utilized the module by identifying threats like impervious surfaces and farmland and setting their intensity and impact distance based on local context and the literature [68,69]. The structure of the equation is expressed as follows:

$$Q_{ab} = H_b \left[1 - \frac{D_{ab}^Z}{D_{ab}^Z + k^z} \right] \tag{9}$$

$$D_{ab} = \sum_{i=1}^{R} \sum_{b=1}^{B_r} \left(\omega_i / \sum_{i=1}^{R} \omega_i \right) i_y j_{iaab} \beta_j S_{bi} \tag{10}$$

$$i_{rab} = 1 - (d_{ab} / d_{r\max}) \tag{11}$$

where Q_{ab} represents the index assessing habitat quality in land use category b at grid a; k represents the semi-saturation coefficient; H_b represents land use category j of habitat suitability; D_{ab} represents the level of habitat decline for grid a; and Z is the default setting, the value of which is set to 2.5. Stressors are variables causing strain; R represents their count; B_r depicts the total number of stress-affected grid cells; ω_i reflects the significance of each stressor; i_y denotes the quantity of stressors within a grid cell; β_j signifies the accessibility rating of grid x; S_{bi} indicates how sensitive land-use type b is to stressors, ranging from 0 to 1; and j_{iab} represents the maximum distance over which stressors exert influence. d_{ab} denotes the Euclidean distance between entity a and entity b, while $d_{r\max}$ signifies the maximum influence range of stressor r.

(4) Carbon Storage (CS)

The carbon storage [70–72] of terrestrial ecosystems (C_{total}) comprises the following four distinct carbon compartments: underground CS (C_{under}), above-ground CS (C_{above}), soil–organic CS (C_{soil}), and dead organic matter CS (C_{dead}). The equation is expressed as follows:

$$C_{\text{total}} = C_{\text{dead}} + C_{\text{above}} + C_{\text{under}} + C_{\text{soil}} \tag{12}$$

2.3.3. Valuation of Ecosystem Service Value (ESV)

The equivalent value coefficient table approach is the most commonly used method in ESV valuation. Initially, Costanza calculated the global ESV using equivalence coefficients [1]. To align with the specific unique characteristics of Chinese ecosystems, Xie adapted the equivalency coefficient table [73]. Therefore, we updated the table for Panzhihua based on the above research. The ESV for impervious surfaces was excluded and assigned a value of zero, as previous research has shown it to be minimal. Next, we determined the standard equivalent factor for the ESs by utilizing the intrinsic economic worth of food per unit area (at 2020 price levels) for the primary crops (rice, wheat, and maize) between 2000 and 2020. The calculated standard equivalent factor was CNY 1541.17/hm^2. Finally, the table for Panzhihua (Table A1 in Appendix A) provides the ESV in unit area for various land use classifications. The computation process is as listed as follows:

$$\mathrm{E} = \frac{1}{7} \sum_{k=1}^{3} \frac{p_k \times q_k \times m_k}{T} \tag{13}$$

$$ESV = \sum_{j=1}^{11} \sum_{i=1}^{7} E \times A_i \times E_{ij} \tag{14}$$

where E represents ESV per ha (CNY/ha); the average marketplace cost of the food crop is labeled as k (CNY/t); q_k represents the mean unit yield of k food crops (t/ha); m_k represents the mean area planted with k food crops (t/ha); T represents the total coverage of food crops; i represents the specific ES and A_i represents the LULC area of ES i in hectares (hm^2); ESV represents total ESVs (CNY); and E_{ij} represents the coefficient that quantifies the ESV for land use j.

2.3.4. Statistical Analysis

(1) Analysis of Correlation

This study performed Spearman correlation analysis, a commonly employed approach, to determine the relationship between pairs of ESs [74,75]. Specifically, grid-scale correlations [76,77] were calculated using the Spearman correlation coefficient. The correlation coefficient [78] is calculated as follows:

$$r_{12} = \frac{\sum_{w=1}^{j}\left(ES_{1(w)} - \overline{ES}_{1(w)}\right)\left(ES_{2(w)} - \overline{ES}_{2(w)}\right)}{\sqrt{\sum_{w=1}^{j}\left(ES_{1(w)} - \overline{ES}_{1(w)}\right)^2 \sum_{j=1}^{j}\left(ES_{2(w)} - \overline{ES}_{2(w)}\right)^2}} \quad (15)$$

where r_{12} represents the correlation coefficient between ESs, $ES_{1(w)}$ represents the first ES at grid w, $\overline{ES}_{1(w)}$ represents the mean level of the first ES at grid w, $ES_{2(w)}$ represents the second ES at grid w, and $\overline{ES}_{2(w)}$ represents the mean level of the second ES at grid w. Trade-off interactions are shown by negative correlations and passing the significance test, while synergy relationships between pairs of ESs are indicated by positive correlations and passing the significance test. The relationship becomes stronger as the absolute value of r_{12} increases.

(2) Identification of Ecosystem Service Bundles

K-means clustering algorithm analysis, an unsupervised approach, compares and gathers high-similarity ESs [23–27]. All of the ESs need to be standardized to a value of 0 to 1 [79] to reduce the impact of units before clustering analysis. Subsequently, a grid of 1 km × 1 km [14] was generated with ArcGIS Pro 3.1 software's Create Fishnet tool. The average ES values were then extracted and assigned as ES sample values inside the grid. The ideal number of clusters was found based on the Calinski criterion using the provided data [80].

3. Results

3.1. LULC from 2000 to 2050

The coefficients of the obtained FoM, OA, and kappa were 0.149, 0.802, and 0.76, respectively. Thus, the verified outcomes demonstrated that the PLUS model possessed significant credibility and could be employed for forecasting of future LULC. Results of the simulation in 2050 under the three investigated scenarios (ND, EP, and FP) are shown in Figure 3. Moreover, a Sankey diagram was used to demonstrate land use transfer changes (Figure 4).

Between 2000 and 2020, most of the area was used for arable land and forests, accounting for over 80 % of the total area, as shown in Figure 4a. The farmland and impervious areas increased, whereas barren, forest, and grassland areas consistently declined. Farmland was mainly converted from forest and grassland. Impervious surfaces showed a clear expansion trend, with a growth rate of 80% between 2000 and 2010. They were predominantly converted from farmland and grassland due to industrialization and urbanization.

The LULC for 2020 was simulated based on LULC data from 2000 and 2010 using the PLUS model, then compared with actual LULC data for 2020. The obtained coefficients of the FoM, OA, and kappa were 0.149, 0.802, and 0.76, respectively. Thus, the verified outcomes demonstrated that the PLUS model possessed significant credibility and could be employed for the forecasting of future LULC. Following this, we simulated the spatial distribution of LULC in 2050 (Figure 3), and the results under different scenarios exhibited significant variations.

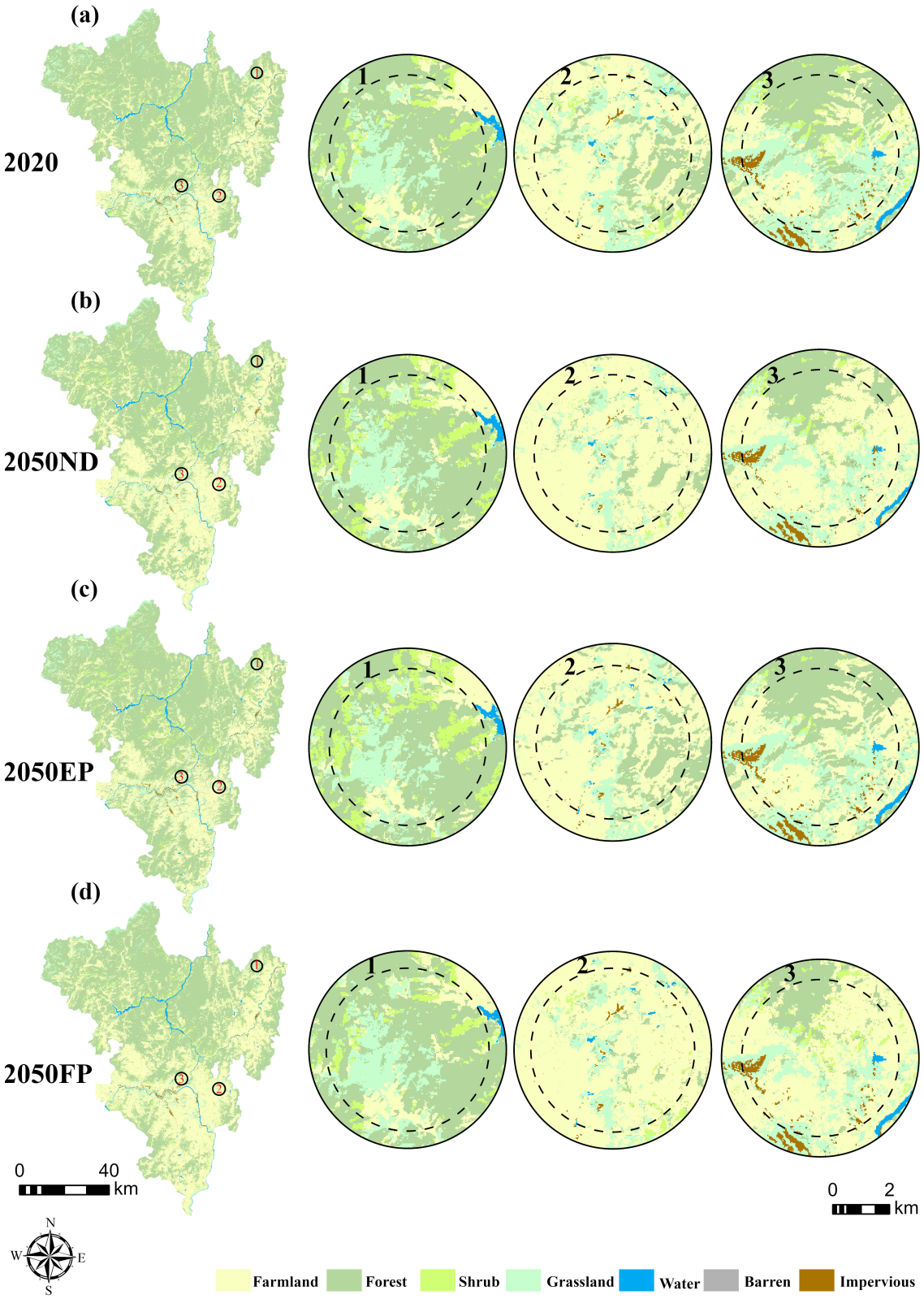

Figure 3. LULC from 2020 to 2050. (**a**) LULC in 2020; (**b**) LULC under the ND scenario in 2050; (**c**) LULC under the EP scenario in 2050; (**d**) LULC under the FP scenario in 2050.1, 2, 3: enlarged images of different areas respectively.

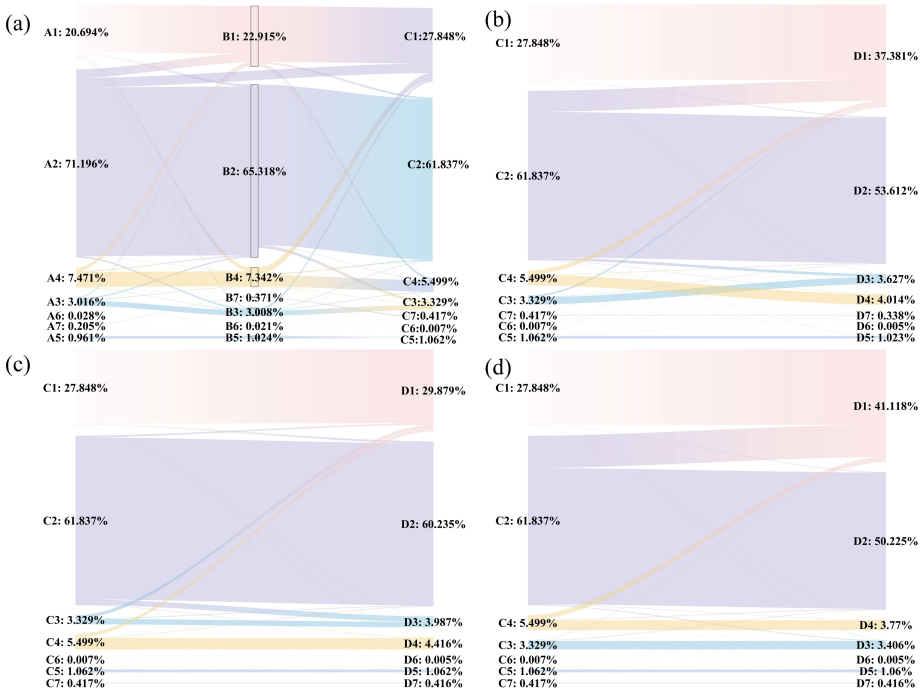

Figure 4. Sankey diagram of LULC transition for 2000–2050. A: 200; B: 2010; C: 2020; D: 2050; 1–7: farmland, forest, shrub, grassland, water, barren, and impervious, respectively. Note: (**a**) 2000–2020; (**b**) 2020—the ND scenario in 2050; (**c**) 2020 – the EP scenario in 2050; (**d**) 2020 – the FP scenario in 2050.

The percentage of farmland area under the three scenarios (ND, EP, and FP) was projected to rise to different extents, namely 37.381%, 29.879%, and 41.118%, respectively (Figure 4b–d). Meanwhile, the expanse of forest and grassland is anticipated to persist in diminishing. Forest will be predominantly found in the northern and middle part of Panzhihua city. The northeastern and southern–central areas will possess the most extensive expanse of farmland. Impervious surfaces will be predominantly distributed in the central and northern regions near water bodies, with their area showing a gradual decline. Forest area will account for 53.612% of the total under the ND scenario, with much of the forest in the southwest being encroached upon by farmland. Existing farmland will expand outward, mainly in areas adjacent to water bodies. Under the EP scenario, however, the forest area will see little change compared to the other two scenarios and remain nearly constant. Farmland in the southern region will expand compared to 2020. Ecological protection policies will impose more stringent restrictions on the expansion of farmland and impervious surfaces in comparison to the ND scenario. There will be a sharp decline in both forested and grassland areas under the FP scenario, with a significant percentage of these areas being converted to farmland. Much of the eastern region will be also occupied by farmland. Farmland expansion will primarily occur in regions with a dense distribution of forests extending in all directions from the original farmland.

3.2. Analysis of Changes in ESs and ESV

3.2.1. ESs Changes

Based on an analysis of the overall distribution of pixels, spatial distribution, and yearly variations in ecosystem services (Figure 5), we deduced substantial changes in the four ecosystem services, with distinct spatial characteristics.

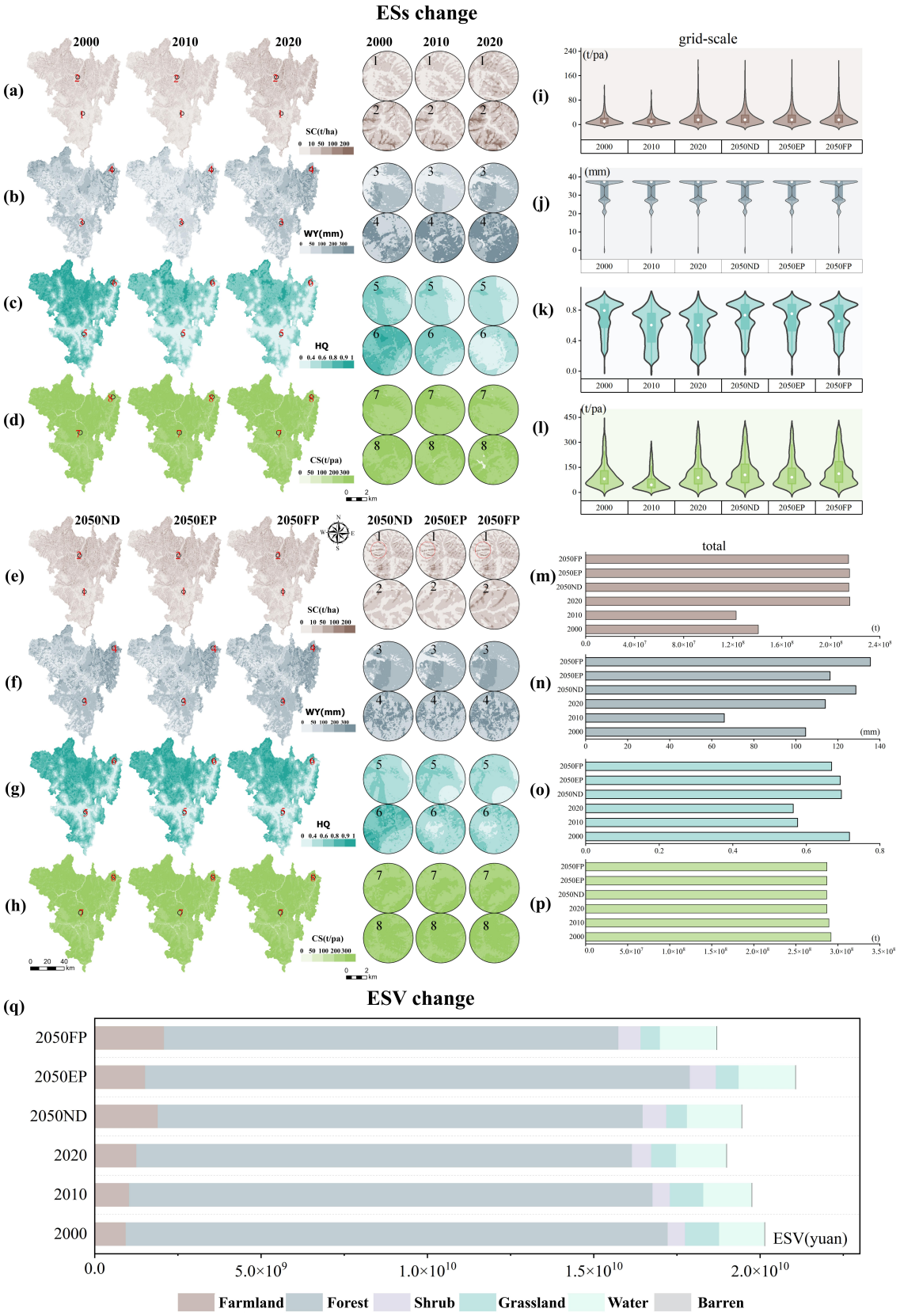

Figure 5. ESs and ESV changes from 2000 to 2050: (**a**–**h**), (**i**–**l**), (**m**–**p**) spatial distribution, overall pixel distribution, and total changes in SC, WY, HQ, and CS, respectively; (**q**) ESV change across different land use categories. 1–8: enlarged images of different areas respectively.

The total SC dropped from 2000 to 2010, followed by a rise from 2010 to 2020. The overall trend indicated a net increase, with values at the grid scale showing a slight upward trend. The center, northern, and eastern edges of had higher levels of SC, whereas the southeastern region had the minimal SC. The annual WY trends were similar to those seen in SC, with the northeast area displaying higher WY values. The CS kept shrinking. The northern region exhibited higher storage compared to the southern region, while the central region boasted the highest storage. HQ consistently worsened. The middle and northern regions exhibited higher levels of HQ, showing similarities to the spatial distribution of CS. During 2000–2020, these ESs showed some fluctuations in both total quantity and grid scale. However, the spatial distribution patterns of the four ESs (Figure 5a–h) largely remained consistent from 2000 to 2050, with only slight changes occurring in specific regions.

ESs exhibit various kinds of change throughout the three different scenarios. CS will continue to exhibit a declining pattern. The decline in CS will be mostly concentrated in the developed region of Panzhihua city. The CS will greatly reduce under the EP scenario, with the slightest decline in CS under the FP scenario. All scenarios will result in an increase in HQ, with the EP scenario resulting in the greatest increase. There will be no notable change in SC at either the grid scale or in the overall amount under any policy. The WY will also show growth in 2050, with the largest annual WY under the FP scenario.

3.2.2. ESV Changes

Total ESVs were estimated (Figure 5q), and they varied among LULC types. From 2000 to 2050, the LULC type with the highest value was forest, followed by farmland. From 2000 to 2020, the total ESVs fell from about CNY 201.412 million to CNY 189.945 million due to the significant reduction in high-value forest, mostly resulting from its conversion into lower-value farmland and impervious surfaces. By 2050, the total ESVs will demonstrate an upward trend compared to 2020 under the ND and EP scenarios. However, they will exhibit a declining tendency under the FP scenario. Under the EP scenario, total ESVs will be higher than under the ND scenario, which will result in greater total ESVs relative to the ND scenario, largely owing to the higher ecosystem service value of forests. Grassland, forests and bodies of water with a high ESV have a particular influence on regional ESV fluctuations.

3.3. Trade-Offs, Synergies, and Bundling of ESs

3.3.1. Trade-Offs and Synergies among ESs during 2000–2050

The correlation coefficients were computed and are shown using a correlation heat map (Figure 6). During 2000–2020, CS had a stable and highly significant positive relationship with HQ ($r > 0.5, p \leq 0.001$), and the r value of this pair gradually decreased. This meant a decline in the synergistic relationship between HQ and CS. However, CS had a negative correlation with WY ($r \leq 0.6, p \leq 0.001$), indicating a clear trade-off between CS and WY. The results proved a clear positive relationship between SC and both HQ and CS, suggesting synergy between them. The synergistic correlation between SC and HQ decreased, as indicated by a decrease in the r value from 0.21 to 0.19. There existed a weak negative correlation between SC and WY, with the absolute value of r remaining at a lower level. By 2050, the trade-off between HQ and WY will enhance and become the strongest in the FP scenario. The r values of CS and HQ will steadily rise under the ND and EP scenarios, implying that the synergistic relationship between them would be further strengthened. In contrast, the synergistic relationship will be weakened under the FP scenario. The trade-off between HQ and WY will gradually weaken under three scenarios.

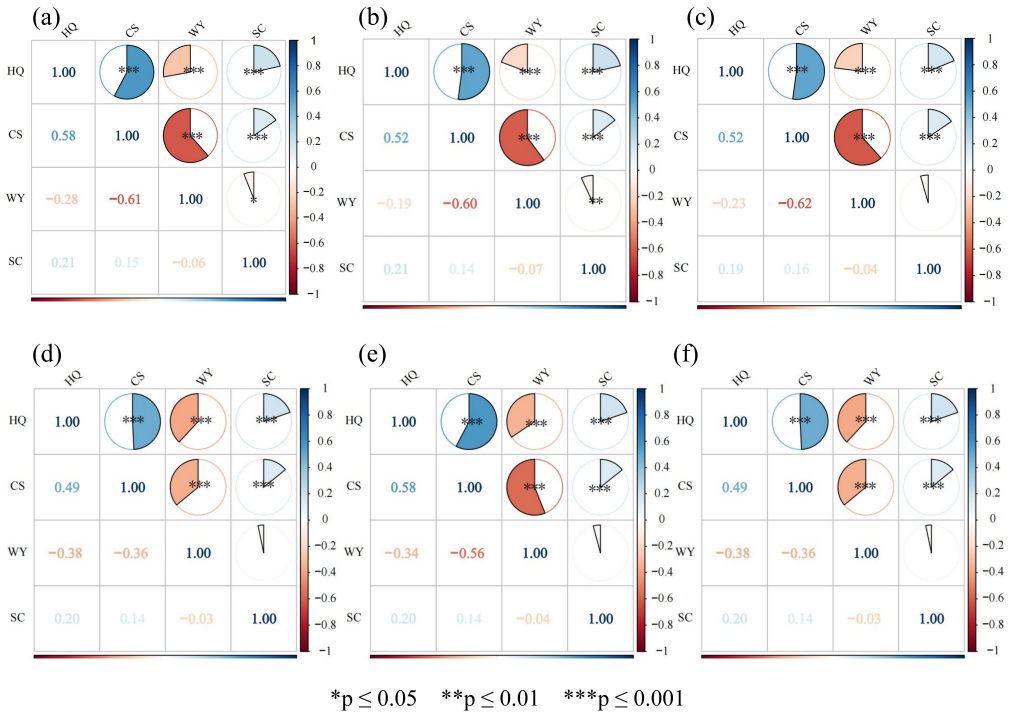

Figure 6. Correlation of ecosystem services: (**a**) 2000; (**b**) 2010; (**c**) 2020; (**d**) ND scenario in 2050; (**e**) EP scenario in 2050; (**f**) FP scenario in 2050.

3.3.2. Spatiotemporal Distribution of ESBs during 2000–2050

Four ESBs, namely, ESB1, ESB2, ESB3, and ESB4, were identified in this study, and Figure 7a displays the compositional structure of the four ESBs. Between 2000 and 2050, there were complex and significant distinctions in the spatial distribution patterns of ESBs (Figure 7b). Among the four ESBs, the level of carbon storage continuously remained high in Panzhihua. ESB1, the ecosystem vulnerability bundle, was represented by a generally low level of ESs. It occupied more than 40% of the area in 2020, decreasing but remaining the greatest percentage of the area by 2050. ESB1 mostly converted from ESB2. ESB2, the soil erosion bundle, had high degrees of CS and HQ and the lowest level of SC compared to all other bundles. It dominated the area proportion from 2000 to 2020, peaking at over 60% in 2010. ESB2 often occurred in proximity to agricultural land and urban areas. ESB3, the ecological balance bundle, offered an abundance of resources from SC, WY, HQ, and CS. Moreover, the mean values of SC and WY were greater than those in other ESBs. From 2000 to 2020, it converted to other bundles and accounted for a tiny proportion of area. However, the proportion of ESB3 was set to rise to 18%. It could be found mainly in areas with dense vegetation and ecological reserves. In ESB4, CS and HQ were the prevailing ESs, with the average value of HQ being equal to or greater than 0.57. ESB4 was mostly discovered in the north–central area of the region. Notably, under three scenarios, transformation will differ among ESBs (Figure 7c). From 2020 to 2050, ESB2 will convert to either ESB1 or ESB3. ESB2, ESB3, and ESB4 will all undergo conversion to ESB1. Among the conversions, the largest number of bundles will be transformed from ESB2 to ESB1. This transformation will be inhibited under the FP scenario. In the EP scenario, ESB2 will be converted into ESB4, while the reverse will occur in the other two scenarios.

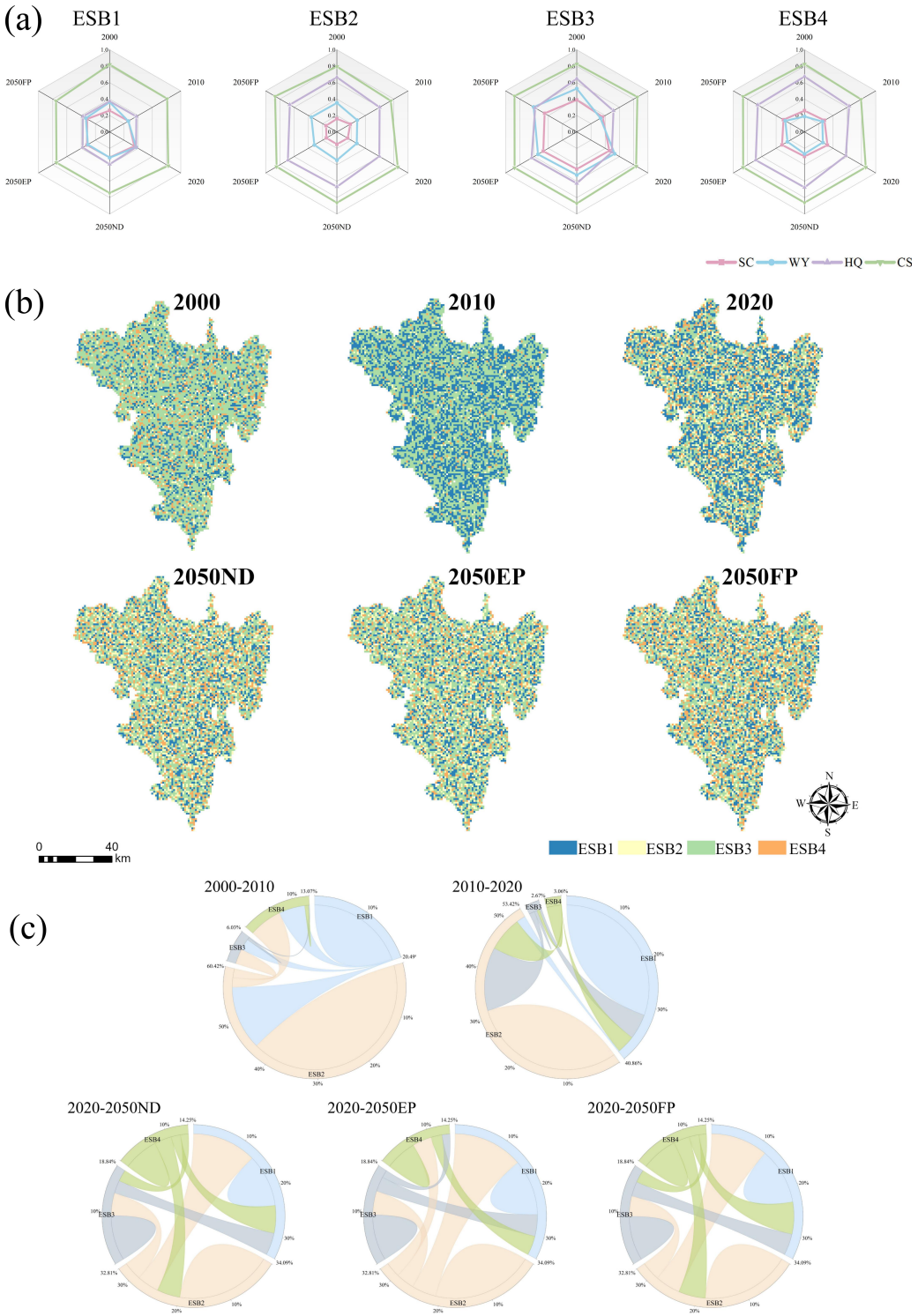

Figure 7. Spatial distribution and temporal changes of the ESBs during 2000–2050: (**a**) compositional structure of ESBs; (**b**) spatial distribution of ESBs; (**c**) chord diagram of ESB transfer.

3.4. Changes in Interactions among Mining Ecosystem Services

We applied correlation analysis to find out the interactions between ESs in various ESBs and further understand the complicated interactions among ESs, as shown in Table 2. We selected nine typical minerals (coal, iron, building sand, shale, limestone, copper or nickel ore, granite, dolomite, and clay) in Panzhihua to study how their extraction impacts ecosystem service interactions across different mining areas (Figure 8).

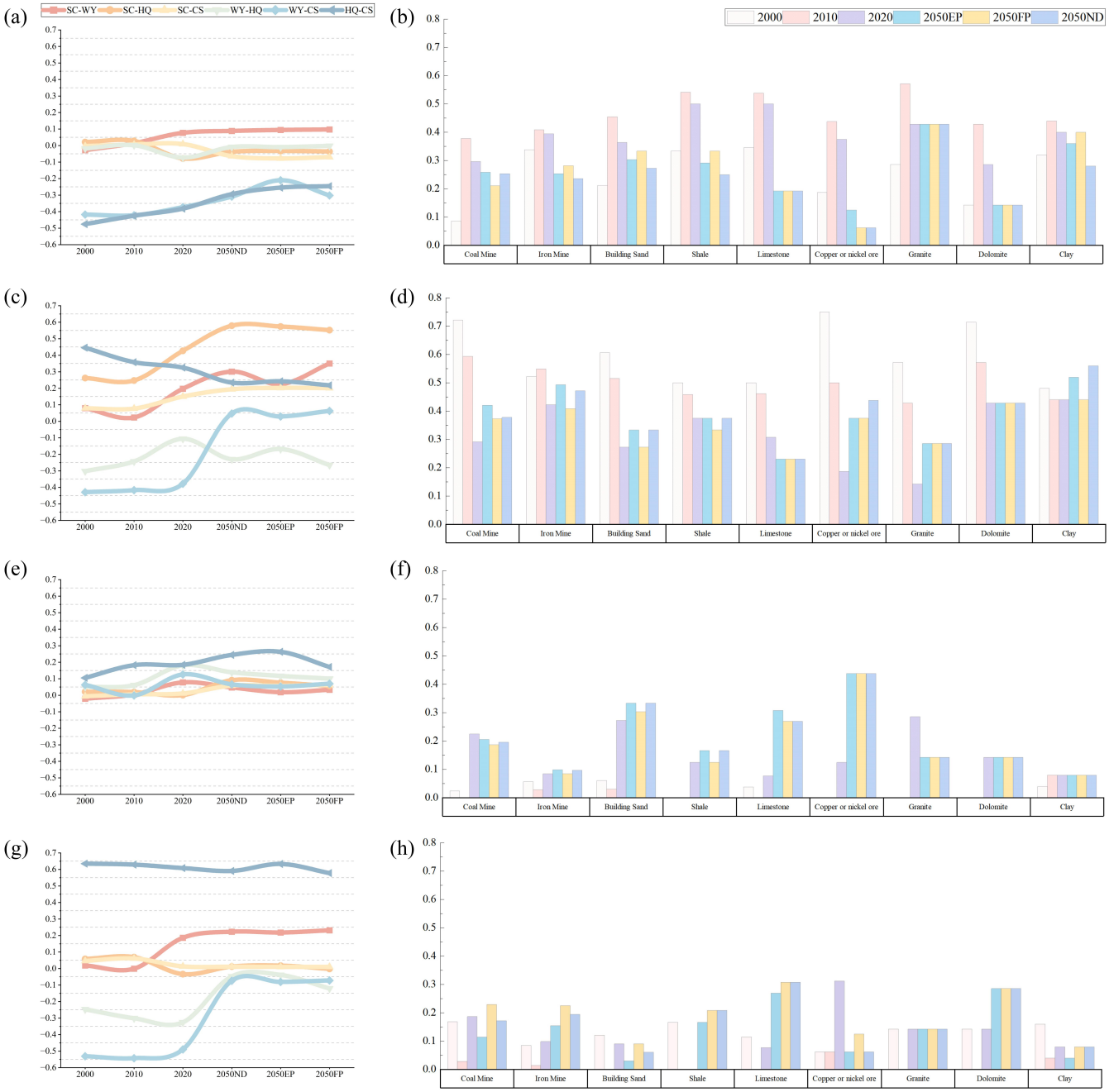

Figure 8. Changes in interactions among mining ESs during 2000–2050: (**a**,**c**,**e**,**g**) correlation coefficient changes of pair of ESs, namely ESB1, ESB2, ESB3, and ESB4, respectively; (**b**,**d**,**f**,**h**) proportions of different mineral types under ESB1, ESB2, ESB3, and ESB4, respectively.

In ESB1, the HQ–CS interactions exhibited a strong trade-off. However, the r value of other pairs of ESs were all close to 0, suggesting an overall non-significantly weak trade-off/synergy relationship. In ESB2, SC had significant synergistic relationships with WY, HQ, and CS. There will also exist synergies among all four of them that will continue to grow stronger by 2050. The synergy between HQ and CS was anticipated to diminish over the period of 2000–2050. In ESB3, there was a significant synergy between WY and HQ, except in 2020. In ESB4, compared to other ESBs, HQ and WY exhibited the most pronounced synergistic relationship.

The interactions among ESs in different mining areas revealed temporal and spatial variations to a certain extent. From 2000 to 2010, the mining areas presented the highest values of the soil erosion bundle (ESB2), exceeding 40%. The quantity of ESB3 was minimal in the mining areas. ESB3 did not appear in shale, granite and dolomite, copper, or nickel mining areas. This damage additionally altered the synergies among different ESs. The quantity of ESB4 found in mining areas for building sand, shale, limestone, granite, and dolomite declined to zero in the year 2010. Between 2010 and 2020, there was a progressive increase in ESB1 in the mining area as ESB2 consistently fell. The granite mining areas had the most notable decline in the amount of ESB2, whereas iron mines showed no substantial change. The ecological balance bundle (ESB3) rose in all areas, excluding coal mines. The shale mining areas had no ESB3, while its values slowly increased in the remaining areas. By 2050, the percentage of ESB1 is projected to decline, whereas the percentages of ESB3 and ESB4 are anticipated to keep increasing. Anticipated growth of ESB2 is projected for all mining areas, with the exception of limestone mines. Among all of the scenarios, ESB2 will have the smallest proportion under the FP scenario. Overall, the mining area will experience a stronger reinforcement of its synergistic relationship as the amount of ESB3 grows in Panzhihua.

Table 2. Interaction of ESs in various ESBs during 2000–2050.

r		2000	2010	2020	2050ND	2050EP	2050FP
ESB1	SC-WY	−0.028	0.014	0.077 **	0.088 **	0.094 **	0.097 **
	SC-HQ	0.021	0.028	−0.078 **	−0.038 *	−0.033	−0.036 *
	SC-CS	−0.003	0.006	0.009	−0.064 **	−0.078 **	−0.07**
	WY-HQ	−0.018	0.002	−0.073 **	−0.009	−0.01	−0.002
	WY-CS	−0.418 **	−0.422 **	−0.373 **	−0.309 **	−0.210 **	−0.302 **
	HQ-CS	−0.476 **	−0.425 **	−0.382 **	−0.294 **	−0.255 **	−0.246 **
ESB2	SC-WY	0.08 **	0.023	0.197 **	0.301 **	0.225 **	0.35 **
	SC-HQ	0.262 **	0.247 **	0.427 **	0.579 **	0.574 **	0.552 **
	SC-CS	0.079 **	0.077 **	0.15 **	0.194 **	0.202 **	0.201 **
	WY-HQ	−0.302 **	−0.243 **	−0.106 **	−0.23 **	−0.168 **	−0.265 **
	WY-CS	−0.429 **	−0.417 **	−0.378 **	0.047 **	0.029	0.063 **
	HQ-CS	0.446 **	0.358 **	0.325 **	0.234 **	0.242 **	0.218 **
ESB3	SC-WY	−0.021	0.005	0.078 **	0.047 **	0.018	0.033 **
	SC-HQ	0.021	0.019	0.001	0.091 **	0.076 **	0.056 **
	SC-CS	−0.006	0.005	0.011	0.058 **	0.057 **	0.063 **
	WY-HQ	0.05 **	0.061 **	0.181 **	0.139 **	0.117 **	0.1 **
	WY-CS	0.063 **	−0.001	0.126 *	0.066 **	0.053 **	0.07 **
	HQ-CS	0.105 **	0.182 **	0.184 **	0.244 **	0.263 **	0.171 **
ESB4	SC-WY	0.018	−0.001	0.186 **	0.223 **	0.218 **	0.231 **
	SC-HQ	0.058 **	0.069 **	−0.034 *	0.012	0.017	−0.002
	SC-CS	0.046 **	0.061 **	0.013	0.011	0.01	0.01
	WY-HQ	−0.247 **	−0.301 **	−0.326 **	−0.048 **	−0.039 **	−0.121**
	WY-CS	−0.531 *	−0.543 **	−0.490 **	−0.074 **	−0.081 **	−0.072**
	HQ-CS	0.635 **	0.629 **	0.608 **	0.591 **	0.633 *	0.578 **

* $p \leq 0.5$; ** $p \leq 0.01$.

4. Discussion

4.1. Significance and Valuation of the ESVs

The significance of ESVs as an essential tool in improving the development of land use has been extensively acknowledged. This study estimated ESVs to further quantify the ESs of mining cities. This enabled a comprehensive assessment of ecological assets, visually depicting the impacts of LULC on ESs across various policy scenarios [4,81,82]. Our study employed the equivalent coefficient table approach, which is favored for its straightforwardness and the broad accessibility of land use data [83]. We enhanced the accuracy ESV estimation by modifying the equivalence factor table developed by Xie [4,73,84] to reflect the specific conditions of Panzhihua [85–87]. The results showed a steady decrease

in total ESVs during 2000–2020. The main factor driving this trend was the loss of the areas dominated by high-value vegetation, coupled with the ongoing expansion of farmland and impervious surfaces. The ND scenario that seeks to emulate historical patterns of land use was projected to witness an enhancement in ESVs by 2050. Under the FP scenario, the encroachment of farmland into high-value vegetation cover areas will lead to a persistent decrease in their future ESVs. The EP scenario will be distinguished by possessing the greatest ESVs among the three estimated scenarios. Panzhihua city is currently facing environmental degradation difficulties. Increasing the coverage of high-value vegetation is considered a significant measure for enhancing its ESVs.However, heightened vegetation cover can elevate evapotranspiration rates, consequently diminishing water availability and impacting both humans and animals. It is paramount to understand the various stages of natural ecological succession. The initial stages, such as those succeeding major disruptions like mining, are frequently seen as periods of environmental degradation. Subsequent stages, such as the establishment of a forested state, are characterized by the flourishing of valuable vegetation [88]. Therefore, acknowledging the differing focal points and expectations associated with each stage is crucial in formulating strategies to improve ecological efficiency [89].

4.2. Impacts of LULC on ESs

LULC directly affects terrestrial ecosystem patterns, processes, and functions [90]. During 2000–2020, there was an apparent trend of diminishing HQ and CS resulting from the decline in forest area and expansion of farmland. This discovery is in agreement with the results reported by Shao et al. [91] and Li et al. [92]. Meanwhile, the synergy between HQ and CS became weakened. It is anticipated that HQ will undergo a significant improvement by 2050. This enhancement will be the most pronounced under the EP scenario, while the synergistic relationship between HQ and CS is expected to intensify. Conversely, this relationship between HQ and CS will continue to diminish under the FP scenario. WY and SC exhibit fluctuating trends. Most studies indicate that evapotranspiration is lower in grasslands relative to forests and shrubs [93–95], so grasslands can produce greater water yield while preserving a relatively high degree of other ESs [96]. However, in our study, farmland and forest were found to be the largest land uses in Panzhihua, reducing the influence of grasslands on the WY of the area. In addition, it was discerned that water yield appears to be more significantly impacted by other factors, such as precipitation levels. WY is anticipated to exacerbate the trade-off with HQ, with the EP scenario poised to mitigate the exacerbation of this trade-off. Minimizing trade-offs among diverse ESs is critical for the formulation of LULC policy and management tactics. Our results show that the EP scenario can efficiently mitigate trade-offs and augment synergies in Panzhihua. Hence, it is imperative for Panzhihua to prioritize the execution of ecological protection regulations with the goal of achieving sustainable local growth in the future.

4.3. Multiple ES Interactions: Trade-Offs and Synergies across Various ESBs

We found substantial disparities in the relationships of ESs among various ESBs. For example, HQ and CS revealed an extreme trade-off interaction in the ecosystem vulnerability bundle (ESB1), yet they exhibited significant synergies across all other service bundles. The synergistic interaction between HQ and CS in ESB4 was the most apparent across the entire region. Meanwhile, we found a synergy between WY and CS in ESB3, in line with prior studies carried out by Wu et al. [79] and Li et al. [30]. Within ESB2 and ESB4, WY and HQ demonstrated a notable trade-off relationship. The trade-off between HQ and WY was also evident in research executed by Yang et al. [97]. In ESB4, the trade-off between WY and HQ intensified during 2000–2020 but is predicted to diminish by 2050. Moreover, the synergy between HQ and CS is expected to strengthen further from 2000 to 2050, particularly under the EP scenario.

4.4. Investigating Variations in Interactions among Mining ESs Based on Mineral Type

It was noticed that there were distinctions in the distributions of ESBs between the mining areas and the Panzhihua region as a whole. During 2000–2020, the soil erosion bundle (ESB2) was the most common ecosystem service bundle in the whole region. As a result of mining activities, most mining areas in Panzhihua also had the largest amount of the soil erosion bundle and the lowest level of soil conservation. However, ESB2 was significantly reduced in the granite, copper, and nickel mining areas. This suggests that soil loss from mining areas such as granite may be minimal [98,99]. The ecosystem vulnerability bundle (ESB1) will have the biggest area in 2050. However, it will decrease in all mining areas, most of all under the EP scenario. The presence of increased ecosystem balance bundles (ESB3) in iron ore, building sand, shale, limestone, and copper or nickel ore mining areas may indicate progress in the ecological restoration of these sites. By focusing on these regions, valuable insights can be gained to guide future ecological protection efforts in the area. Moreover, the synergy between SC and other ecosystem services in mining regions is poised for further enhancement, propelled by a rise in ESB3 counts. Consequently, Panzhihua's mine rehabilitation policy is anticipated to produce tangible results, suggesting that future strategies should emphasize the promotion of eco-friendly mining activities.

4.5. Limitations and Prospects

This research makes a significant contribution by exploring the complex interactions among ESs across different mineral types and analyzing their distinctions. However, it also recognizes certain limitations. Discrepancies in the spatial resolution of data, such as carbon pools and climatic variables, introduce potential inaccuracies. This underscores the need for future refinement in parameter accuracy and data resolution to improve ecosystem service evaluations. This study's scope is further constrained by the availability of precise mining intensity data, limiting our exploration of mining impacts on comprehensive ecosystem services. Future research should integrate more detailed mining data and biophysical metrics to deepen our understanding of the formation and evolution mechanisms driving ecosystem service bundles in mining cities. Mining areas labeled as disadvantaged may also cultivate valuable ecological resources, thereby offering crucial inspiration for conservation and planning initiatives [100]. This will enable the development of more scientifically grounded and effective ecological management strategies for the region, reducing the limitations of the current research and expanding its future applicability.

5. Conclusions

In this study, we incorporated the PLUS-InVEST model in combination with Spearman correlation and the K-means clustering algorithm to project and analyze future LULC and ES dynamics in a representative mining city. Our findings are summarized as follows: (1) In Panzhihua, farmland and forest dominated land use, with total ESVs declining during 2000–2020 due to increases in farmland and impervious surfaces. By 2050, the ecological protection scenario will curb forest loss, enhancing these values, while farmland expansion under the farmland protection scenario will further reduce them. (2) Four ecosystem bundles were identified, with the soil erosion bundle predominating between 2000 and 2020. By 2050, the ecosystem vulnerability bundle is predicted to dominate under all scenarios. The ecological protection scenario will improve the synergy between habitat quality and carbon storage. But the farmland protection scenario will exacerbate the trade-off between habitat quality and water yield. (3) The distribution of ecosystem service bundles in Panzhihua's mining area diverged from the region at large, with notable declines in the soil erosion bundle from 2000 to 2020. The ecosystem vulnerability bundle of mining areas is projected to decrease, especially under the ecological protection scenario in 2050, which will also strengthen the synergies between soil conservation and other ecosystem services.

This study integrates an analysis of changes in ESBs to examine ES interactions across mineral types under various policy scenarios. It establishes a theoretical foundation for

future ecosystem management in mining cities, aiming to achieve a harmonious coexistence between mineral resource exploitation and long-term environmental preservation.

Author Contributions: Conceptualization, X.P. and X.D.; Data curation, Y.Z. (Yujian Zheng); Formal analysis, X.P.; Funding acquisition, X.D. and W.L.; Methodology, X.P., X.D. and Y.Z. (Yang Zhang); Resources, X.D., Y.Z. (Yujian Zheng) and W.L.; Software, Y.Z. (Yujian Zheng); Supervision, Y.Z. (Yang Zhang), J.W. and H.H.; Validation, X.L., Y.X., J.W. and H.H.; Visualization, X.P.; Writing—original draft, X.P. and X.D.; Writing—review and editing, R.S. and W.L. All authors have read and agreed to the published version of the manuscript.

Funding: This work is supported by the State Key Laboratory of Geohazard Prevention and Geoenvironment Protection Independent Research Project (Grant No. SKLGP2022Z007), as well as the Key Research and Development Program of Sichuan Province (Grant No. 2023YFS0435).

Data Availability Statement: The original contributions presented in the study are included in the article, further inquiries can be directed to the corresponding author.

Conflicts of Interest: The authors declare no conflicts of interest.

Appendix A

Table A1. ESVs per unit area of various land use categories in Panzhihua (CNY/hm^2).

Primary Categorization	Secondary Categorization	Farmland	Forest	Shrub	Grassland	Water	Barren
Provisioning services	Supply of food	1702.99	421.25	292.82	359.61	1232.94	0
	Raw ingredient	377.59	970.94	662.7	529.14	354.47	0
	Provision of water	−2011.23	503.45	339.06	292.82	12,776.31	0
Regulating services	Regulation of gas	1371.64	3195.36	2173.05	1859.68	1186.7	30.82
	Regulation of climate	716.64	9555.26	6519.15	4916.33	3529.28	0
	Cleanse the environment	208.06	2779.24	1972.7	1623.37	8553.5	154.12
	Hydrological Regulation	2304.05	5954.06	5162.92	3601.2	157,569.3	46.24
Supporting services	Formation and preservation of soil	801.41	3888.89	2650.81	2265.52	1433.29	30.82
	Maintaining nutrient cycling	238.88	297.96	200.35	174.67	107.88	0
	Conservation of biodiversity	262	3539.56	2419.64	2060.03	3929.99	30.82
Cultural services	Entertainment and Culture	115.59	1551.45	1063.41	909.29	2912.81	15.41

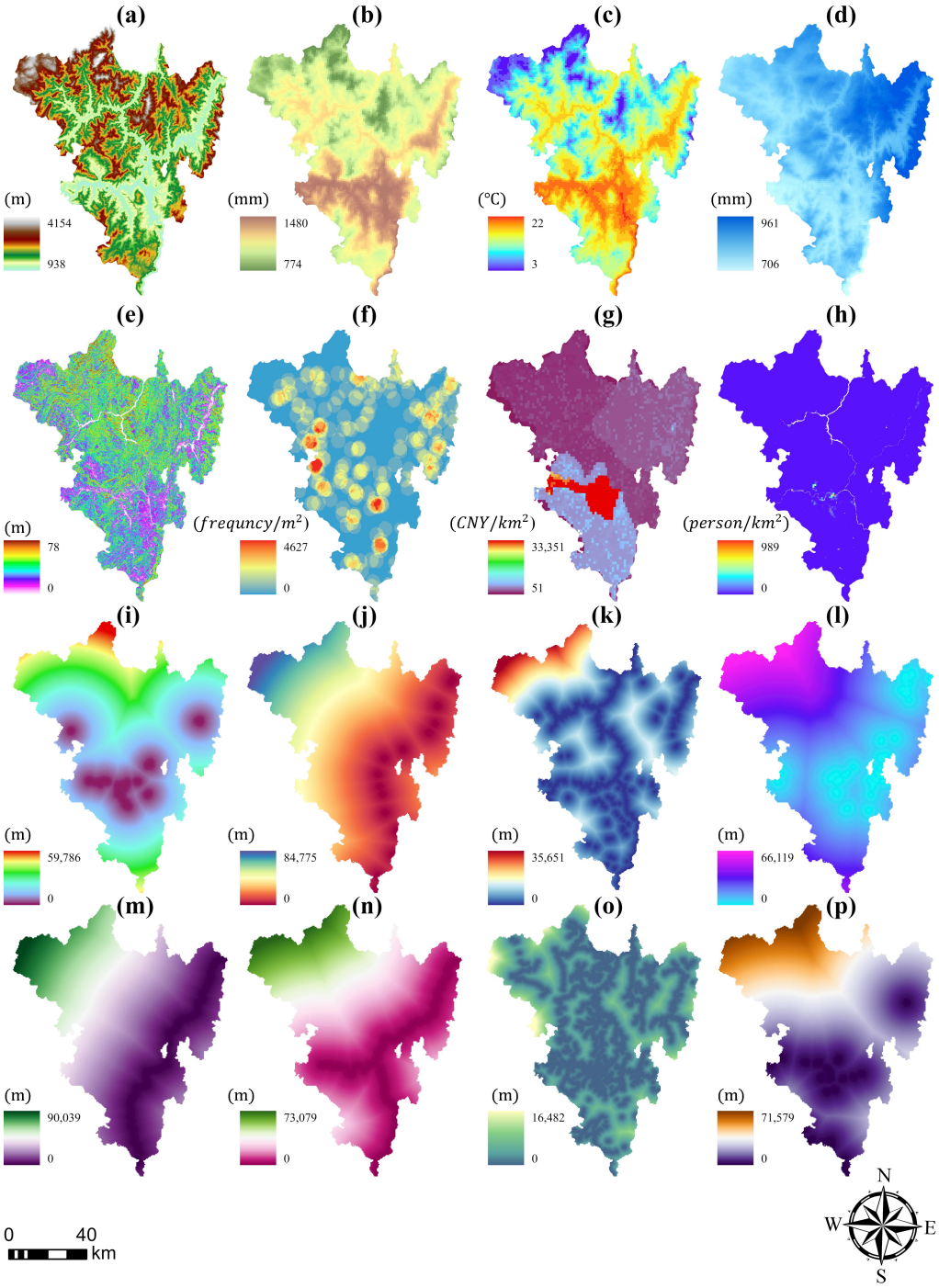

Figure A1. Driving factors: (**a**) DEM; (**b**) Evapotranspiration; (**c**) Mean yearly temperature; (**d**) Mean yearly rainfall; (**e**) Slope; (**f**) Disaster point density; (**g**) GDP; (**h**) Population density; (**i**) Distance to government; (**j**) Distance to railway station; (**k**) Distance to waterbodies; (**l**) Distance to the mining areas; (**m**) Distance to highway; (**n**) Distance to railway; (**o**) Distance to secondary road; (**p**) Distance to tertiary road.

References

1. Costanza, R.; d'Arge, R.; de Groot, R.; Farber, S.; Grasso, M.; Hannon, B.; Limburg, K.; Naeem, S.; O'Neill, R.V.; Paruelo, J.; et al. The value of the world's ecosystem services and natural capital. *Ecol. Econ.* **1998**, *25*, 3–15. [CrossRef]
2. Daily, G.; Postel, S.; Bawa, K.; Kaufman, L. *Nature's Services: Societal Dependence On Natural Ecosystems*; Island Press: Chicago, IL, USA, 1997; pp. 1–10.
3. Kareiva, P.; Watts, S.; McDonald, R.; Boucher, T. Domesticated nature: Shaping landscapes and ecosystems for human welfare. *Science* **2007**, *316*, 1866–1869. [CrossRef] [PubMed]
4. Xie, G.; Zhang, C.; Zhang, C.; Xiao, Y.; Lu, C. The value of ecosystem services in China. *Resour. Sci.* **2015**, *37*, 1740–1746. [CrossRef]
5. Jopke, C.; Kreyling, J.; Maes, J.; Koellner, T. Interactions among ecosystem services across Europe: Bagplots and cumulative correlation coefficients reveal synergies, trade-offs, and regional patterns. *Ecol. Indic.* **2015**, *49*, 46–52. [CrossRef]
6. Cord, A.F.; Bartkowski, B.; Beckmann, M.; Dittrich, A.; Hermans-Neumann, K.; Kaim, A.; Lienhoop, N.; Locher-Krause, K.; Priess, J.; Schroeter-Schlaack, C.; et al. Towards systematic analyses of ecosystem service trade-offs and synergies: Main concepts, methods and the road ahead. *Ecosyst. Serv.* **2017**, *28*, 264–272. [CrossRef]
7. Bradford, J.B.; D'Amato, A.W. Recognizing trade-offs in multi-objective land management. *Front. Ecol. Environ.* **2012**, *10*, 210–216. [CrossRef] [PubMed]
8. Lin, S.; Wu, R.; Yang, F.; Wang, J.; Wu, W. Spatial trade-offs and synergies among ecosystem services within a global biodiversity hotspot. *Ecol. Indic.* **2018**, *84*, 371–381. [CrossRef]
9. Rodriguez, J.P.; Beard, T.; Douglas, J.; Bennett, E.M.; Cumming, G.S.; Cork, S.J.; Agard, J.; Dobson, A.P.; Peterson, G.D. Trade-offs across space, time, and ecosystem services. *Ecol. Soc.* **2006**, *11*, 28. [CrossRef]
10. Zhang, Z.; Liu, Y.; Zhang, Y.; Liu, Y.; Lu, Y.; Ren, Q. Spatial Non-Stationary Response of the Ecosystem Services Synergy and Tradeoff to Influencing Factors:A Case Study of Ecological Function Area in Fujian Province. *Geomat. Inf. Sci. Wuhan Univ.* **2022**, *47*, 111–125. [CrossRef]
11. Raudsepp-Hearne, C.; Peterson, G.D.; Bennett, E.M. Ecosystem service bundles for analyzing tradeoffs in diverse landscapes. *Proc. Natl. Acad. Sci. USA* **2010**, *107*, 5242–5247. [CrossRef]
12. Spake, R.; Lasseur, R.; Crouzat, E.; Bullock, J.M.; Lavorel, S.; Parks, K.E.; Schaafsma, M.; Bennett, E.M.; Maes, J.; Mulligan, M.; et al. Unpacking ecosystem service bundles: Towards predictive mapping of synergies and trade-offs between ecosystem services. *Glob. Environ. Change-Human Policy Dimens.* **2017**, *47*, 37–50. [CrossRef]
13. Agudelo, C.A.R.; Bustos, S.L.H.; Moreno, C.A.P. Modeling interactions among multiple ecosystem services. A critical review. *Ecol. Model.* **2020**, *429*, 109103. [CrossRef]
14. Turner, K.G.; Odgaard, M.V.; Bocher, P.K.; Dalgaard, T.; Svenning, J.C. Bundling ecosystem services in Denmark: Trade-offs and synergies in a cultural landscape. *Landsc. Urban Plan.* **2014**, *125*, 89–104. [CrossRef]
15. Yang, H.; Zhong, X.; Deng, S.; Xu, H. Assessment of the impact of LUCC on NPP and its influencing factors in the Yangtze River basin, China. *Catena* **2021**, *206*, 105542. [CrossRef]
16. Xiao, S.; Wu, W.; Guo, J.; Ou, M.; Pueppke, S.G.; Ou, W.; Tao, Y. An evaluation framework for designing ecological security patterns and prioritizing ecological corridors: Application in Jiangsu Province, China. *Landsc. Ecol.* **2020**, *35*, 2517–2534. [CrossRef]
17. Bhatta, B.; Shrestha, S.; Shrestha, P.K.; Talchabhadel, R. Evaluation and application of a SWAT model to assess the climate change impact on the hydrology of the Himalayan River Basin. *Catena* **2019**, *181*, 104082. [CrossRef]
18. Abbaspour, K.C.; Rouholahnejad, E.; Vaghefi, S.; Srinivasan, R.; Yang, H.; Klove, B. A continental-scale hydrology and water quality model for Europe: Calibration and uncertainty of a high-resolution large-scale SWAT model. *J. Hydrol.* **2015**, *524*, 733–752. [CrossRef]
19. Zhang, K.; Tang, X.; Zhao, Y.; Huang, B.; Huang, L.; Liu, M.; Luo, E.; Li, Y.; Jiang, T.; Zhang, L.; et al. Differing perceptions of the youth and the elderly regarding cultural ecosystem services in urban parks: An exploration of the tour experience. *Sci. Total Environ.* **2022**, *821*, 153388. [CrossRef] [PubMed]
20. Nelson, E.; Mendoza, G.; Regetz, J.; Polasky, S.; Tallis, H.; Cameron, D.R.; Chan, K.M.A.; Daily, G.C.; Goldstein, J.; Kareiva, P.M.; et al. Modeling multiple ecosystem services, biodiversity conservation, commodity production, and tradeoffs at landscape scales. *Front. Ecol. Environ.* **2009**, *7*, 4–11. [CrossRef]
21. Dittrich, A.; Seppelt, R.; Vaclavik, T.; Cord, A.F. Integrating ecosystem service bundles and socio-environmental conditions—A national scale analysis from Germany. *Ecosyst. Serv.* **2017**, *28*, 273–282. [CrossRef]
22. Lyu, R.; Clarke, K.C.; Zhang, J.; Feng, J.; Jia, X.; Li, J. Spatial correlations among ecosystem services and their socio-ecological driving factors: A case study in the city belt along the Yellow River in Ningxia, China. *Appl. Geogr.* **2019**, *108*, 64–73. [CrossRef]
23. Gao, J.; Yu, Z.; Wang, L.; Vejre, H. Suitability of regional development based on ecosystem service benefits and losses: A case study of the Yangtze River Delta urban agglomeration, China. *Ecol. Indic.* **2019**, *107*, 105579. [CrossRef]
24. Gou, M.; Li, L.; Ouyang, S.; Wang, N.; La, L.; Liu, C.; Xiao, W. Identifying and analyzing ecosystem service bundles and their socioecological drivers in the Three Gorges Reservoir Area. *J. Clean. Prod.* **2021**, *307*, 127208. [CrossRef]
25. Liu, Y.; Lu, Y.; Fu, B.; Harris, P.; Wu, L. Quantifying the spatio-temporal drivers of planned vegetation restoration on ecosystem services at a regional scale. *Sci. Total Environ.* **2019**, *650*, 1029–1040. [CrossRef] [PubMed]
26. Queiroz, C.; Meacham, M.; Richter, K.; Norstrom, A.V.; Andersson, E.; Norberg, J.; Peterson, G. Mapping bundles of ecosystem services reveals distinct types of multifunctionality within a Swedish landscape. *Ambio* **2015**, *44*, S89–S101. [CrossRef] [PubMed]

27. Zhang, Y.; Lu, X.; Liu, B.; Wu, D.; Fu, G.; Zhao, Y.; Sun, P. Spatial relationships between ecosystem services and socioecological drivers across a large-scale region: A case study in the Yellow River Basin. *Sci. Total Environ.* **2021**, *766*, 142480. [CrossRef]
28. Orsi, F.; Ciolli, M.; Primmer, E.; Varumo, L.; Geneletti, D. Mapping hotspots and bundles of forest ecosystem services across the European Union. *Land Use Pol.* **2020**, *99*, 104840. [CrossRef]
29. Hsieh, C.H.; Lin, H.W.; Liu, W.Y. Assessing the ecosystem services provided by conventional and organic farmlands: A better outcome for organic farmlands? *Ecosyst. Serv.* **2023**, *60*, 101514. [CrossRef]
30. Li, S.; Zhao, Y.; Xiao, W.; Yellishetty, M.; Yang, D. Identifying ecosystem service bundles and the spatiotemporal characteristics of trade-offs and synergies in coal mining areas with a high groundwater table. *Sci. Total Environ.* **2022**, *807*, 151036. [CrossRef]
31. Liu, J.; Pei, X.; Zhu, W.; Jiao, J. Scenario modeling of ecosystem service trade-offs and bundles in a semi-arid valley basin. *Sci. Total Environ.* **2023**, *896*, 166413. [CrossRef]
32. Paudel, S.; States, S.L. Urban green spaces and sustainability: Exploring the ecosystem services and disservices of grassy lawns versus floral meadows. *Urban For. Urban Green.* **2023**, *84*, 127932. [CrossRef]
33. Hasan, S.S.; Zhen, L.; Miah, M.G.; Ahamed, T.; Samie, A. Impact of land use change on ecosystem services: A review. *Environ. Dev.* **2020**, *34*, 100527. [CrossRef]
34. Liu, Y.; Tong, Z.; Liu, S.; Huang, D. Progress and Prospects of Research on Optimal Land-Use Allocation Modeling. *Geomat. Inf. Sci. Wuhan Univ.* **2022**, *47*, 1598–1614. [CrossRef]
35. Tolessa, T.; Senbeta, F.; Kidane, M. The impact of land use/land cover change on ecosystem services in the central highlands of Ethiopia. *Ecosyst. Serv.* **2017**, *23*, 47–54. [CrossRef]
36. Zhang, M.; Dai, Z.; Bouma, T.J.; Bricker, J.; Townend, I.; Wen, J.; Zhao, T.; Cai, H. Tidal-flat reclamation aggravates potential risk from storm impacts. *Coast. Eng.* **2021**, *166*, 103868. [CrossRef]
37. Wang, Z.; Li, X.; Mao, Y.; Li, L.; Wang, X.; Lin, Q. Dynamic simulation of land use change and assessment of carbon storage based on climate change scenarios at the city level: A case study of Bortala, China. *Ecol. Indic.* **2022**, *134*, 108499. [CrossRef]
38. Zhang, Y.; Li, Y.; Lv, J.; Wang, J.; Wu, Y. Scenario simulation of ecological risk based on land use/cover change-A case study of the Jinghe county, China. *Ecol. Indic.* **2021**, *131*, 108176. [CrossRef]
39. Li, X.; Chen, G.; Liu, X.; Liang, X.; Wang, S.; Chen, Y.; Pei, F.; Xu, X. A New Global Land-Use and Land-Cover Change Product at a 1-km Resolution for 2010 to 2100 Based on Human-Environment Interactions. *Ann. Am. Assoc. Geogr.* **2017**, *107*, 1040–1059. [CrossRef]
40. Liu, X.; Liang, X.; Li, X.; Xu, X.; Ou, J.; Chen, Y.; Li, S.; Wang, S.; Pei, F. A future land use simulation model (FLUS) for simulating multiple land use scenarios by coupling human and natural effects. *Landsc. Urban Plan.* **2017**, *168*, 94–116. [CrossRef]
41. Wang, H.; Stephenson, S.R.; Qu, S. Modeling spatially non-stationary land use/cover change in the lower Connecticut River Basin by combining geographically weighted logistic regression and the CA-Markov model. *Int. J. Geogr. Inf. Sci.* **2019**, *33*, 1313–1334. [CrossRef]
42. Su, Y.; Ma, X.; Feng, Q.; Liu, W.; Zhu, M.; Niu, J.; Liu, G.; Shi, L. Patterns and controls of ecosystem service values under different land-use change scenarios in a mining-dominated basin of northern China. *Ecol. Indic.* **2023**, *151*, 110321. [CrossRef]
43. Liang, X.; Guan, Q.; Clarke, K.C.; Liu, S.; Wang, B.; Yao, Y. Understanding the drivers of sustainable land expansion using a patch-generating land use simulation (PLUS) model: A case study in Wuhan, China. *Comput. Environ. Urban Syst.* **2021**, *85*, 101569. [CrossRef]
44. Gaur, S.; Singh, R. A Comprehensive Review on Land Use/Land Cover (LULC) Change Modeling for Urban Development: Current Status and Future Prospects. *Sustainability* **2023**, *15*, 903. [CrossRef]
45. Magliocca, N.R.; Dhungana, P.; Sink, C.D. Review of counterfactual land change modeling for causal inference in land system science. *J. Land Use Sci.* **2023**, *18*, 1–24. [CrossRef]
46. Ericsson, M.; Löf, O. Mining's contribution to national economies between 1996 and 2016. *Miner. Econ.* **2019**, *32*, 223–250. [CrossRef]
47. Kumi, S.; Addo-Fordjour, P.; Fei-Baffoe, B. Mining-induced changes in ecosystem services value and implications of their economic and relational cost in a mining landscape, Ghana. *Heliyon* **2023**, *9*, e21156. [CrossRef] [PubMed]
48. Castello, L.; Macedo, M.N. Large-scale degradation of Amazonian freshwater ecosystems. *Glob. Chang. Biol.* **2016**, *22*, 990–1007. [CrossRef]
49. Boldy, R.; Santini, T.; Annandale, M.; Erskine, P.D.; Sonter, L.J. Understanding the impacts of mining on ecosystem services through a systematic review. *Extr. Ind. Soc.* **2021**, *8*, 457–466. [CrossRef]
50. Sonter, L.J.; Herrera, D.; Barrett, D.J.; Galford, G.L.; Moran, C.J.; Soares-Filho, B.S. Mining drives extensive deforestation in the Brazilian Amazon. *Nat. Commun.* **2017**, *8*, 1013. [CrossRef]
51. Zhang, M.; Schwarz, C.; Lin, W.; Naing, H.; Cai, H.; Zhu, Z. A new perspective on the impacts of Spartina alterniflora invasion on Chinese wetlands in the context of climate change: A case study of the Jiuduansha Shoals, Yangtze Estuary. *Sci. Total Environ.* **2023**, *868*, 161477. [CrossRef]
52. Xiang, H.; Wang, Z.; Mao, D.; Zhang, J.; Zhao, D.; Zeng, Y.; Wu, B. Surface mining caused multiple ecosystem service losses in China. *J. Environ. Manag.* **2021**, *290*, 112618. [CrossRef] [PubMed]
53. Jiao, W.; Zhang, X.; Li, C.; Guo, J. Sustainable transition of mining cities in China: Literature review and policy analysis. *Resour. Policy* **2021**, *74*, 101867. [CrossRef]

54. Wang, Z.; Lechner, A.M.; Yang, Y.; Baumgartl, T.; Wu, J. Mapping the cumulative impacts of long-term mining disturbance and progressive rehabilitation on ecosystem services. *Sci. Total Environ.* **2020**, *717*, 137214. [CrossRef] [PubMed]
55. Li, L.; Lei, Y.; Wu, S.; He, C.; Yan, D. Study on the coordinated development of economy, environment and resource in coal-based areas in Shanxi Province in China: Based on the multi-objective optimization model. *Resour. Policy* **2018**, *55*, 80–86. [CrossRef]
56. Wen, B.; Pan, Y.; Zhang, Y.; Liu, J.; Xia, M. Does the Exhaustion of Resources Drive Land Use Changes? Evidence from the Influence of Coal Resources-Exhaustion on Coal Resources-Based Industry Land Use Changes. *Sustainability* **2018**, *10*, 2698. [CrossRef]
57. Dai, X.; Gao, Y.; He, X.; Liu, T.; Jiang, B.; Shao, H.; Yao, Y. Spatial-temporal pattern evolution and driving force analysis of ecological environment vulnerability in Panzhihua City. *Environ. Sci. Pollut. Res.* **2021**, *28*, 7151–7166. [CrossRef] [PubMed]
58. Peng, S. *1 km Monthly Potential Evapotranspiration Dataset in China (1901–2022)*; National Tibetan Plateau Data Center: Beijing, China, 2022. [CrossRef]
59. Du, S.; Zhou, Z.; Huang, D.; Zhang, F.; Deng, F.; Yang, Y. The Response of Carbon Stocks to Land Use/Cover Change and a Vulnerability Multi-Scenario Analysis of the Karst Region in Southern China Based on PLUS-InVEST. *Forests* **2023**, *14*, 2307. [CrossRef]
60. Xu, C.; Zhang, Q.; Yu, Q.; Wang, J.; Wang, F.; Qiu, S.; Ai, M.; Zhao, J. Effects of land use/cover change on carbon storage between 2000 and 2040 in the Yellow River Basin, China. *Ecol. Indic.* **2023**, *151*, 110345. [CrossRef]
61. Varga, O.G.; Pontius, R.; Gilmore, J.; Singh, S.K.; Szabo, S. Intensity Analysis and the Figure of Merit's components for assessment of a Cellular Automata - Markov simulation model. *Ecol. Indic.* **2019**, *101*, 933–942. [CrossRef]
62. Deng, Z.; Quan, B.; Zhang, H.; Xie, H.; Zhou, Z. Scenario Simulation of Land Use and Cover under Safeguarding Ecological Security: A Case Study of Chang-Zhu-Tan Metropolitan Area, China. *Forests* **2023**, *14*, 2131. [CrossRef]
63. Bai, Y.; Ochuodho, T.O.; Yang, J. Impact of land use and climate change on water-related ecosystem services in Kentucky, USA. *Ecol. Indic.* **2019**, *102*, 51–64. [CrossRef]
64. Gao, J.; Li, F.; Gao, H.; Zhou, C.; Zhang, X. The impact of land-use change on water-related ecosystem services: A study of the Guishui River Basin, Beijing, China. *J. Clean. Prod.* **2017**, *163*, S148–S155. [CrossRef]
65. Yohannes, H.; Soromessa, T.; Argaw, M.; Dewan, A. Impact of landscape pattern changes on hydrological ecosystem services in the Beressa watershed of the Blue Nile Basin in Ethiopia. *Sci. Total Environ.* **2021**, *793*, 148559. [CrossRef] [PubMed]
66. Aneseyee, A.B.; Noszczyk, T.; Soromessa, T.; Elias, E. The InVEST Habitat Quality Model Associated with Land Use/Cover Changes: A Qualitative Case Study of the Winike Watershed in the Omo-Gibe Basin, Southwest Ethiopia. *Remote Sens.* **2020**, *12*, 1103. [CrossRef]
67. Wu, L.; Sun, C.; Fan, F. Estimating the Characteristic Spatiotemporal Variation in Habitat Quality Using the InVEST Model-A Case Study from Guangdong-Hong Kong-Macao Greater Bay Area. *Remote Sens.* **2021**, *13*, 1008. [CrossRef]
68. Fu, B.; Xu, P.; Wang, Y.; Guo, Y. Integrating Ecosystem Services and Human Demand for a New Ecosystem Management Approach: A Case Study from the Giant Panda World Heritage Site. *Sustainability* **2020**, *12*, 295. [CrossRef]
69. Xie, X.; Zhu, Q. Research on the Impact of Urban Expansion on Habitat Quality in Chengdu. *Sustainability* **2023**, *15*, 6271. [CrossRef]
70. Babbar, D.; Areendran, G.; Sahana, M.; Sarma, K.; Raj, K.; Sivadas, A. Assessment and prediction of carbon sequestration using Markov chain and InVEST model in Sariska Tiger Reserve, India. *J. Clean. Prod.* **2021**, *278*, 123333. [CrossRef]
71. Liu, Q.; Yang, D.; Cao, L.; Anderson, B. Assessment and Prediction of Carbon Storage Based on Land Use/Land Cover Dynamics in the Tropics: A Case Study of Hainan Island, China. *Land* **2022**, *11*, 244. [CrossRef]
72. Tian, L.; Tao, Y.; Fu, W.; Li, T.; Ren, F.; Li, M. Dynamic Simulation of Land Use/Cover Change and Assessment of Forest Ecosystem Carbon Storage under Climate Change Scenarios in Guangdong Province, China. *Remote Sens.* **2022**, *14*, 2330. [CrossRef]
73. Xie, G.; Zhang, C.; Zhang, L.; Chen, W.; Li, S. Improvement of the Evaluation Method for Ecosystem Service Value Based on Per Unit Area. *J. Nat. Resour.* **2015**, *30*, 1243–1254. [CrossRef]
74. Su, C.h.; Fu, B.J.; He, C.S.; Lü, Y.H. Variation of ecosystem services and human activities: A case study in the Yanhe Watershed of China. *Acta Oecol. Int. J. Ecol.* **2012**, *44*, 46–57. [CrossRef]
75. Zeng, J.; Xu, J.; Li, W.; Dai, X.; Zhou, J.; Shan, Y.; Zhang, J.; Li, W.; Lu, H.; Ye, Y.; et al. Evaluating Trade-Off and Synergies of Ecosystem Services Values of a Representative Resources-Based Urban Ecosystem: A Coupled Modeling Framework Applied to Panzhihua City, China. *Remote Sens.* **2022**, *14*, 5282. [CrossRef]
76. Gao, X.J.; Gray, J.M.; Reich, B.J. Long-term, medium spatial resolution annual land surface phenology with a Bayesian hierarchical model. *Remote Sens. Environ.* **2021**, *261*, 112484. [CrossRef]
77. Zhang, J.; Li, S.; Lin, N.; Lin, Y.; Yuan, S.; Zhang, L.; Zhu, J.; Wang, K.; Gan, M.; Zhu, C. Spatial identification and trade-off analysis of land use functions improve spatial zoning management in rapid urbanized areas, China. *Land Use Pol.* **2022**, *116*, 106058. [CrossRef]
78. Dai, X.; Fan, W.; Shan, Y.; Gao, Y.; Liu, C.; Nie, R.; Zhang, D.; Li, W.; Zhang, L.; Sun, X.; et al. LAI-Based Phenological Changes and Climate Sensitivity Analysis in the Three-River Headwaters Region. *Remote Sens.* **2022**, *14*, 3748. [CrossRef]
79. Wu, L.; Sun, C.; Fan, F. Multi-criteria framework for identifying the trade-offs and synergies relationship of ecosystem services based on ecosystem services bundles. *Ecol. Indic.* **2022**, *144*, 109453. [CrossRef]
80. Zhang, T.; Zhang, S.; Cao, Q.; Wang, H.; Li, Y. The spatiotemporal dynamics of ecosystem services bundles and the social-economic-ecological drivers in the Yellow River Delta region. *Ecol. Indic.* **2022**, *135*, 108573. [CrossRef]

81. Daily, G.C.; Söderqvist, T.; Aniyar, S.; Arrow, K.; Dasgupta, P.; Ehrlich, P.R.; Folke, C.; Jansson, A.; Jansson, B.O.; Kautsky, N.; et al. Ecology. The value of nature and the nature of value. *Science* **2000**, *289*, 395–396. [CrossRef]
82. Egoh, B.; Rouget, M.; Reyers, B.; Knight, A.T.; Cowling, R.M.; van Jaarsveld, A.S.; Welz, A. Integrating ecosystem services into conservation assessments: A review. *Ecol. Econ.* **2007**, *63*, 714–721. [CrossRef]
83. Peng, K.; Jiang, W.; Ling, Z.; Hou, P.; Deng, Y. Evaluating the potential impacts of land use changes on ecosystem service value under multiple scenarios in support of SDG reporting: A case study of the Wuhan urban agglomeration. *J. Clean. Prod.* **2021**, *307*. [CrossRef]
84. Xie, G.; Lin, Z.; Chun-xia, L.U.; Yu, X.; Cao, C. Expert Knowledge Based Valuation Method of Ecosystem Services in China. *J. Nat. Resour.* **2008**, *23*, 911–919. [CrossRef]
85. Ge, G.; Zhang, J.; Chen, X.; Liu, X.; Hao, Y.; Yang, X.; Kwon, S. Effects of land use and land cover change on ecosystem services in an arid desert-oasis ecotone along the Yellow River of China. *Ecol. Eng.* **2022**, *176*, 106512. [CrossRef]
86. He, C.; Shao, H.; Xian, W. Spatiotemporal Variation and Driving Forces Analysis of Eco-System Service Values: A Case Study of Sichuan Province, China. *Int. J. Environ. Res. Public Health* **2022**, *19*, 8595. [CrossRef] [PubMed]
87. Tan, Z.; Guan, Q.; Lin, J.; Yang, L.; Luo, H.; Ma, Y.; Tian, J.; Wang, Q.; Wang, N. The response and simulation of ecosystem services value to land use/land cover in an oasis, Northwest China. *Ecol. Indic.* **2020**, *118*, 106711. [CrossRef]
88. Schaaf, W.; Pohle, I.; Maurer, T.; Gerwin, W.; Hinz, C.; Badorreck, A. Water balance dynamics during ten years of ecological development at Chicken Creek catchment. *Vadose Zone J.* **2017**, *16*, 1–14. [CrossRef]
89. Zaplata, M.K.; Winter, S.; Fischer, A.; Kollmann, J.; Ulrich, W. Species-driven phases and increasing structure in early-successional plant communities. *Am. Nat.* **2013**, *181*, E17–E27. [CrossRef] [PubMed]
90. Yuan, X.; Wang, C.; Li, B.; Wang, W.; Chen, N. Review of the Driving Forces and Impacts of Land Use/Cover Change in the Yangtze River Basin. *Geomat. Inf. Sci. Wuhan Univ.* **2023**, *48*, 1241–1255. [CrossRef]
91. Shao, Z.; Chen, C.; Liu, Y.; Cao, J.; Liao, G.; Lin, Z. Impact of Land Use Change on Carbon Storage Based on FLUS-InVEST Model: A Case Study of Chengdu-Chongqing Urban Agglomeration, China. *Land* **2023**, *12*, 1531. [CrossRef]
92. Li, X.; Liu, Z.; Li, S.; Li, Y. Multi-Scenario Simulation Analysis of Land Use Impacts on Habitat Quality in Tianjin Based on the PLUS Model Coupled with the InVEST Model. *Sustainability* **2022**, *14*, 6923. [CrossRef]
93. Madani, E.M.; Jansson, P.E.; Babelon, I. Differences in water balance between grassland and forest watersheds using long-term data, derived using the CoupModel. *Hydrol. Res.* **2018**, *49*, 72–89. [CrossRef]
94. Yang, D.; Liu, W.; Tang, L.; Chen, L.; Li, X.; Xu, X. Estimation of water provision service for monsoon catchments of South China: Applicability of the InVEST model. *Landsc. Urban Plan.* **2019**, *182*, 133–143. [CrossRef]
95. Li, M.; Liang, D.; Xia, J.; Song, J.; Cheng, D.; Wu, J.; Cao, Y.; Sun, H.; Li, Q. Evaluation of water conservation function of Danjiang River Basin in Qinling Mountains, China based on InVEST model. *J. Environ. Manag.* **2021**, *286*, 112212. [CrossRef] [PubMed]
96. Schaaf, W.; Hinz, C.; Gerwin, W.; Zaplata, M.K.; Huettl, R.F. Ecosystem development in the constructed catchment "chicken creek". In *Hydrology of Artificial and Controlled Experiments*; Liu, J.F., Gu, W.Z., Eds.; Books on Demand: Norderstedt, Germany, 2018; pp. 75–93. [CrossRef]
97. Yang, Y.; Li, M.; Feng, X.; Yan, H.; Su, M.; Wu, M. Spatiotemporal variation of essential ecosystem services and their trade-off/synergy along with rapid urbanization in the Lower Pearl River Basin, China. *Ecol. Indic.* **2021**, *133*, 108439. [CrossRef]
98. Hu, X.; Ma, C.; Huang, P.; Guo, X. Ecological vulnerability assessment based on AHP-PSR method and analysis of its single parameter sensitivity and spatial autocorrelation for ecological protection: A case of Weifang City, China. *Ecol. Indic.* **2021**, *125*, 107464. [CrossRef]
99. Vettegren, V.I.; Shcherbakov, I.P.; Voronin, A.V.; Kuksenko, V.S.; Mamalimov, R.I. Dynamics of the deformation and destruction of a heterogeneous body (granite) under the influence of an electric discharge. *Phys. Solid State* **2014**, *56*, 1018–1022. [CrossRef]
100. Zaplata, M.K.; Dullau, S. Applying ecological succession theory to birds in solar parks: An approach to address protection and planning. *Land* **2022**, *11*, 718. [CrossRef]

Disclaimer/Publisher's Note: The statements, opinions and data contained in all publications are solely those of the individual author(s) and contributor(s) and not of MDPI and/or the editor(s). MDPI and/or the editor(s) disclaim responsibility for any injury to people or property resulting from any ideas, methods, instructions or products referred to in the content.